Equivalence Principle in Chameleon Models

Lucila Kraiselburd[1,2,*] Susana J. Landau[2,3,†] Marcelo Salgado[4,‡] Daniel Sudarsky[4,5,§] and Héctor Vucetich[1,¶]

[1]*Grupo de Astrofísica, Relatividad y Cosmología,*
Facultad de Ciencias Astronómicas y Geofísicas, Universidad Nacional de La Plata,
Paseo del Bosque S/N (1900) La Plata, Argentina
[2]*CONICET, Godoy Cruz 2290, 1425 Ciudad Autónoma de Buenos Aires, Argentina*
[3]*Departamento de Física, Facultad de Ciencias Exactas y Naturales,*
Universidad de Buenos Aires and IFIBA, Ciudad Universitaria - Pab. I, Buenos Aires 1428, Argentina
[4]*Instituto de Ciencias Nucleares, Universidad Nacional Autónoma de México, A.P. 70-543, México D.F. 04510, México*
[5]*Department of Philosophy, New York University,*
New York, NY 10003, United States of América
(Dated: April 9, 2018)

Most theories that predict time and/or space variation of fundamental constants also predict violations of the Weak Equivalence Principle (WEP). In 2004 Khoury and Weltman [1] proposed the so called *chameleon field* arguing that it could help avoiding experimental bounds on the WEP while having a non-trivial cosmological impact. In this paper we revisit the extent to which these expectations continue to hold as we enter the regime of high precision tests. The basis of the study is the development of a *new* method for computing the force between *two massive bodies induced by the chameleon field* which takes into account the influence on the field by both, the *large* and the *test* bodies. We confirm that in the *thin shell* regime the force does depend non-trivially on the *test* body's composition, even when the chameleon coupling constants $\beta^i = \beta$ are universal. We also propose a simple criterion based on energy minimization, that we use to determine which of the approximations used in computing the scalar field in a two body problem is better in each specific regime. As an application of our analysis we then compare the resulting differential acceleration of two *test* bodies with the corresponding bounds obtained from Eötvös type experiments. We consider two setups: 1) an Earth based experiment where the *test* bodies are made of Be and Al; 2) the Lunar Laser Ranging experiment. We find that for some choices of the free parameters of the chameleon model the predictions of the Eötvös parameter are larger than some of the previous estimates. As a consequence, we put new constrains on these free parameters. Our conclusions strongly suggest that the properties of immunity from experimental tests of the WEP, usually attributed to the chameleon and related models, should be carefully reconsidered. An important result of our analysis is that our approach leads to new constraints on the parameter space of the chameleon models.

PACS numbers:

I. INTRODUCTION

The Weak Equivalence Principle (WEP) is a cornerstone of the Einstein's Theory of General Relativity (hereafter GR), and can be broadly seen as implying the universal coupling between matter and gravity. That is usually taken as translating directly into the universality of free fall (UFF), and thus as a feature easily analyzed and directly testable. The first point we want to make is that the situation is substantially more complex than previously thought. This is due to the fact that the WEP is, strictly speaking, only meant to hold for test point-like objects (i.e. a principle meant to apply locally) that do not affect the gravitational environment around them. However, in reality no such objects exist in nature, even if the test-point-like assumption is in occasions a good approximation. All objects have, in principle, a non-vanishing energy-momentum tensor, and as such, they all modify the geometry of space-time. Those modifications, in turn, affect the motion of the object themselves. In fact, taking into account the so called "back reaction effects" is a highly nontrivial task (see for instance [2]). Moreover, given that all real objects have a finite spatial extension, one requires, for a rigorous description of their motion, the determination of something akin to the notion of the "center of mass world-line", a task that is highly nontrivial in general space-times [3]. The

*Electronic address: lkrai@fcaglp.unlp.edu.ar
†Electronic address: slandau@df.uba.ar
‡Electronic address: marcelo@nucleares.unam.mx
§Electronic address: sudarsky@nucleares.unam.mx
¶Electronic address: vucetich@fcaglp.unlp.edu.ar

results of the detailed analyses indicate that those world-lines do not, in general, correspond to geodesics. Quantum aspects further complicate the analysis of the motion of even the simplest things, which one might want to take as paradigmatic point like objects, such as photons[4]. Even though such UFF violating effects are normally very small, they are always there in principle, and therefore these considerations should serve as warnings when we go on to analyze more complex situations.

Of particular interest for us here will be any theory in which the local coupling constants are taken to be effectively space-time dependent, while respecting the principles of locality and general covariance, as those entail some kind of fundamental field controlling the spatial dependence, with the field, generically, coupling in different manners to the various types of matter. Such field, usually taken to be a scalar field, generically mediates new forces between *macroscopic* objects, which would look, at the empirical level, as modifications of gravitation which might, in principle, lead to effective violations of the UFF for *test* bodies in external gravitational fields. For this reason, most theories that predict variations of fundamental constants also predict effective violations of the WEP [5–9]. For instance, the rest energy of a macroscopic body is made of many contributions related to the energies associated with various kinds of interactions (strong, weak, electromagnetic) and such components would be affected differently by a light scalar field. From the experimental point of view, one needs to confront the very strong limits on possible violations of the WEP that come from Eötvös-Roll-Krotkov-Dicke and Braginsky-Panov experiments and their modern reincarnations [10–15] which explore the differential acceleration of *test* bodies in gravitational contexts. In fact current bounds reach sensitivities of order $\frac{\Delta a}{a} \simeq 10^{-13}$ (or more), and thus can, in principle, constrain the viability of many models.

Recently, there has been a great level of interest in models that claim to be able to avoid the stringent bounds resulting from experimental tests looking for violations of the WEP based on schemes where the effects of the fields are hidden by suitable non-linearities, as in the chameleon models and the Dilaton-Matter-gravity model with strong coupling [16]. Chameleon models were introduced by Khoury and Weltman in 2004 [1] and have been further developed by several authors [18–25, 27]. Generically a *chameleon* consists of a scalar field that is coupled non-minimally to matter and minimally to the curvature (or the other way around via a conformal transformation), and where the field's effective mass depends on the density and pressure of the matter that constitutes the *environment*. This, in turn, is the result of the nontrivial coupling of the scalar field with the trace of the energy-momentum tensor of the matter sector of the theory [1]. The coupling of the scalar field with matter might be *non-universal* (i.e. it may depend on the particle's species), like in the original model introduced in [1], or universal as in some simpler models.

In their work Khoury and Weltman [1] analyzed the chameleon field associated with a single body using a "linear" approximation in the equation, and corroborated that the corresponding solution looks very similar to the numerical solution of the full non-linear equation

This approximation to the one body problem will be referred hereafter to as *the standard approach* [2]. Their conclusion was that the bounds imposed by the experiments testing the WEP can be satisfied (even if the coupling constants are of order unity) provided that the bodies involved in the relevant experiments generate the so called *thin shell effect*. In this *thin shell* regime, the spatial variations of the scalar field take place just on a small region near the body's surface thus preventing the scalar field from actually exerting any force on most of the body. A further analysis by Mota and Shaw [19] strengthened the conclusion that the non linearities inherent to the chameleon models are, in fact, responsible for suppressing the effective violation of WEP in the actual experiments even when the coupling constants are very large, and not just when they are of order unity as it was initially thought [1] [3]. Moreover, these authors argued that the predicted effective violations of the WEP in low density environments (like in space-based laboratories) would be further suppressed for some adjusted values of the parameters of the scalar-field potential.

Based on such analyses, a good part of the community working on the area [1, 19, 21, 22, 24, 27–30] has come to believe the chameleon fields should not lead to any relevant forces in experiments on Earth designed to search for a dependence on the composition of the acceleration of a falling *test* body, or in general, to any observable interaction between ordinary bodies mediated by chameleon-type fields.

However, it should be noted that there is no universal consensus in the community regarding even qualitative aspects of the theoretical predictions, with some arguments indicating the chameleon force on the *test* body is composition dependent [1, 19, 21, 22, 27–29] and others indicating that it is not [30]. Defining a "screened" *test* body one in which the *thin shell* condition is satisfied and an "unscreened" *test* body one in which it is not satisfied, most authors make

---

[1] In this context by *matter* we mean any field other that the scalar-field at hand, which in the situation of interest would be the ordinary matter making up the objects present in the experiment including the atmosphere.

[2] See Appendix E for a short review of the standard approach for the one body problem and a discussion of the *thin shell* condition

[3] When analyzing the two-body problem, Mota & Shaw [19] assumed that both bodies can be treated as two semi-infinite "blocks" and then solved the non-linear equation for the chameleon. After making several approximations they concluded that the force between the bodies is composition-independent. We thus worried that in such approximations the mass of both bodies would become infinite, and the magnitude of some potentially problematic terms was not estimated.

different predictions on the composition dependence of the chameleon mediated force [1, 19]. It is also important to recall that there are two different expressions for the *thin shell* condition in the literature: the first one offered by Khoury & Weltmann [1] using the linear approximation to the field equation, and the second one, proposed by Mota & Shaw [19], based on considerations of the complete nonlinear equation, and that this latter condition also depends on the value of the environment's density as well as the value of the chameleon potential parameters and that of β.

We do not find the arguments based on the *thin shell* phenomena to be sufficiently persuasive. The basic observation is that one could, equally well, have claimed something not entirely different by considering two macroscopic and charged conductors. It is well known that the mobility of charges in conducting materials ensure that in static situations the charges are distributed on the conductors' surface in such a way that the electric field inside, vanishes exactly. Thus, except for a *thin shell* on the surface of each body, one could have argued (following a similar logic as the one used in the context of the chameleon models), the external electric field could not exert forces on the conductor's material. However, we of course know that large macroscopic forces between such macroscopic bodies are the rule. The resulting force could therefore be attributed solely to the *thin shell* effects.

In view of this, we proceeded to study this issue for the case of the chameleon in more detail, in order to understand what, if any, is the fundamental difference between the two situations (i.e. between the electromagnetic case mentioned above and the one concerning the theory at hand). That is, we want to find out if the *thin shell* arguments are valid at the level of accuracy that would actually ensure the "disappearance" of the expected forces. The basic point is that when the contribution to the scalar field by the presence of the *test* body in an actual experiment is sufficiently large to create a *thin shell* effect, then, the body cannot really be considered as a simple *test* particle, and the problem needs to be treated as a two body problem, i.e., one requires to analyze the full effect of the two bodies on the scalar field in order to evaluate the effective force exerted by the field on the body of interest. The main contribution of this paper consists in analyzing the chameleon field generated by two spherical bodies of finite size (a large one and a smaller one) and the computation of the effective force on the *test* (smaller) body using first principles. To this end a *linear* approximation for the field equation was used in all our analysis. This linear approximation is different from the standard linear approximation used by Khoury and Weltman [1] [4]. As far as we are aware, this approach is novel. Now before moving forward, it is worth stressing two important aspects related to chameleon models: the first one is a matter of principle, and refers to the fact that, effectively the WEP is violated by construction in this kind of models, as opposed to purely metric-based theories (like GR) where the WEP is incorporated *ab initio*. That is, the WEP (for *test point particles* moving on geodesics) is satisfied with infinite precision in purely metric theories of gravity involving no other long range fields coupling to matter. Nevertheless, even in such metric theories the absolute validity of the WEP refers only to *test point particles* which, as stressed above, do not really exist in nature (as a result of Heisenberg's uncertainty principle). In any event, when ignoring those quantum complications, it is clear that the WEP is respected for *point test particles* in metric theories, while, in chameleon models, the WEP is violated a priori (i.e. by construction in models with non-universal coupling) *even* when referring to *point test particles*. As we shall see, this violation can be exacerbated when considering actual *extended test objects*. The second aspect concerns the experiments themselves. Even if chameleon models violate by construction the WEP, those violations might not be observable in a laboratory experiment if the precision is not adequate. This, as is well known, means that some of the effects that might reflect these violations of the WEP can be suppressed by the *thin shell* phenomenon associated with the chameleon field or by the Yukawa dependence of the force associated with the effective mass of the field. Thus, as we shall illustrate, within a framework of a two body problem, these violations of the WEP might be large, in contexts where the two bodies are embedded in a very a light medium (e.g. the vacuum or the air atmosphere) (see Fig. 7 in Sec. V) whereas they could be strongly suppressed when part of the setting (e.g. the *test* body) is encased in some shell of a dense material like a metal vacuum chamber.

In order to explore these issues in detail, we evaluate the static chameleon field associated with two extended spherical bodies, one large and one small, of different chemical composition. For simplicity, only the larger one will be taken to be *the source* of the gravitational field. We shall see that under these and other simplifying assumptions concerning the equation of motion for the chameleon, even when considering a universal coupling and the suppression due to the metal encasing of the experimental setup, violations of the WEP do arise for some values of the chameleon field parameters (see Figs. 9, 10 and 12 in Sec. V). This result, although *previously known*, may seem rather counter-intuitive as in this scenario all the various metrics $g_{\mu\nu}^{(i)}$ coalesce into a single (Jordan) metric $g_{\mu\nu}^{\mathrm{J}}$ (see Sec. II for the details). These violations are then put in perspective with the results found by various authors using different approaches and approximations (see Sec. V).

The paper is organized as follows. After briefly reviewing the original chameleon model in Section II, we present the method for computing the two body problem proposed in this work. Then, in Section III we develop a simple

---

[4] In a future work we plan to analyze other types of approximations which we expect can lead to more accurate solutions.

criterion based on the use of an energy functional for which the minimization corresponds to the field configuration of the physical solution, to determine when the method proposed in this paper is better than the one employed in the standard approach and when it is not. That method is used to identify the range of the model's parameters where our results should be considered as more trustworthy that the results obtained in previous studies. In Section IV we compute the force on the *test* body and show that the force is not negligible and, to the extent that there is no protective symmetry to prevent it, it will lead to an acceleration that depends on the *test* body's composition. In Section V we apply our results to two concrete experiments, the Eöt-Wash torsion balance and the Lunar Laser Ranging (LLR). For the first one, our discussion incorporates the characterization of the outside medium and the effects of the vacuum chamber's encasing shell. In both cases we provide numerical estimates for the Eötvös parameter. In the former case we find that the actual experimental setting generates complications in the numerical part of our analysis. Nevertheless, we provide our estimates for the bounds including rough estimates of the corrections resulting from the specific experimental setup, which we consider can serve as motivation for further analytical and experimental work. For instance, we explore the estimates for the experimental bounds that arise from considering two different modelings for the outside medium. We also explore the modifications that arise from including the effect of the metal shell, showing that in some regimes the violations of the WEP can be significantly suppressed for $\beta > 10^{-2}$ (we are indebted to P. Brax for pointing this specific aspect to us). Finally, in Section VI we present our conclusions and a discussion about their impact on other alternative theories of gravity. Several appendices complete the ideas of the main sections.

II.   THE CHAMELEON MODEL

In this section we briefly review the main aspects of the chameleon model. The model involves a scalar-field φ that couples minimally to gravity via a fiducial metric $g_{\mu\nu}$, according to the following action

$$S[g_{\mu\nu}, \Psi_m^{(i)}, \varphi] = \int d^4x \sqrt{-g} \left[\frac{M_{pl}^2}{2} R - \frac{1}{2} g^{\mu\nu} (\nabla_\mu \varphi)(\nabla_\nu \varphi) - V(\varphi) \right] - \int d^4x L_m \left(\Psi_m^{(i)}, g_{\mu\nu}^{(i)} \right), \tag{1}$$

where $M_{pl} = 1/\sqrt{8\pi}$ is the reduced Planck mass, R is the Ricci scalar associated with $g_{\mu\nu}$, and $\Psi_m^{(i)}$ represents schematically the different matter fields (i.e. the fields other than the chameleon φ; for instance, all the fundamental fields of the standard model of particle physics). The potential $V(\varphi)$ is specified below. The particular feature of this action is that each specie i of matter couples *minimally* to its corresponding metric $g_{\mu\nu}^{(i)}$, while the scalar field φ couples *non-minimally*, and in general, *non-universally* to the matter through a conformal factor that relates each metric $g_{\mu\nu}^{(i)}$ with the so called Einstein metric $g_{\mu\nu}$:

$$g_{\mu\nu}^{(i)} = \exp\left[\frac{2\beta_i \varphi}{M_{pl}} \right] g_{\mu\nu}. \tag{2}$$

Here $g_{\mu\nu}^{(i)}$ is the metric which is usually associated with the geodesics of each specie i of matter and β_i is the corresponding coupling constant between each specie and the chameleon field. For instance, when the coupling constants are universal, $\beta_i = \beta$, then the (universal) metric $g_{\mu\nu}^J = g_{\mu\nu}^{(i)}$ is called the Jordan metric, and then point particles would follow the geodesics of this metric. We will see, however, that a more detailed analysis indicates that even in the universal coupling case, within the relevant experimental situations, that simple conclusion need not apply. Given the fact that, in general, the chameleon field couples differently to each specie of particle, this model leads to potential violations of the WEP that could in principle be explored experimentally.

Following [1, 19, 27], we consider the potential for the chameleon field to be,

$$V(\varphi) = \lambda M^{4+n} \varphi^{-n}, \tag{3}$$

where M is a constant, and n is a free parameter that can be taken to be either a positive integer or a negative even integer [cf. Eq. (12)] ($\lambda = 1$ for all values of n except when $n = -4$ where $\lambda = \frac{1}{4!}$.).

The energy-momentum tensor (EMT), $T_{\mu\nu}^{m(i)}$, for the $i$the matter component can be written in terms of the EMT, $T_{\mu\nu}^m$ associated with the Einstein metric as follows:

$$T_{\mu\nu}^{m(i)} = + \frac{2}{\sqrt{-g^{(i)}}} \frac{\delta L_m}{\delta g_{(i)}^{\mu\nu}} = \exp\left[\frac{-2\beta_i \varphi}{M_{pl}} \right] T_{\mu\nu}^m, \tag{4}$$

where $T_{\mu\nu}^m$ is defined similarly from L_m but using the metric $g_{\mu\nu}$ instead of $g_{\mu\nu}^{(i)}$.

Consequently, the traces of both EMT's are related by

$$T^{m(i)} = g_{(i)}^{\mu\nu} T_{\mu\nu}^{m(i)} = \exp\left[\frac{-4\beta_i\varphi}{M_{pl}}\right] g^{\mu\nu} T_{\mu\nu}^m = \exp\left[\frac{-4\beta_i\varphi}{M_{pl}}\right] T^m. \tag{5}$$

Eventually, we will assume a perfect-fluid description for $T_{\mu\nu}^m$. Specifically, this perfect fluid will be taken to characterize each of two extended bodies, together with the matter constituting the environment, all of which we consider as the "source" of the chameleon field. Furthermore, in the analysis of the resulting force between the two bodies, we will simply consider a universal coupling and set $\beta_i = \beta$, in order to simplify the calculations. Hereafter, and unless otherwise indicated, all the differential operators and tensorial quantities are associated with the Einstein metric.

The equation of motion for the the chameleon φ which arises from the action (1) is

$$\Box\varphi = \frac{\partial V_{\text{eff}}}{\partial\varphi}, \tag{6}$$

where V_{eff} represents the effective potential defined by:

$$V_{\text{eff}} = V(\varphi) - T^m \frac{\beta\varphi}{M_{pl}}, \tag{7}$$

which depends on the energy-density and pressure of the matter fields via T^m. So for the perfect fluid model, $T^m = -\rho + 3P$ which does not depend explicitly on φ.

A. Modelling the experimental setup

As we mentioned earlier, we are interested in the general static solution of Eq. (6) in the presence of two extended bodies that for simplicity we consider as spherical. We take one of them to be a very *large* body of mass $\mathcal{M}$ (e.g. Earth, Sun, a mountain), and the other one is a smaller body of mass $\mathcal{M}_2$ ($\mathcal{M}_2 \ll \mathcal{M}$; hereafter *test* body). Both bodies are the source of the chameleon, and each one is taken to have a different but uniform density, which formally can be represented by suitable Heaviside (step) functions. Moreover, we shall consider the *linear* approximation in Eq. (6) obtained by linearizing Eq. (7) around φ_{min} (associated with the minimum of V_{eff}) in each of the three mediums (i.e. the two bodies and the *environment*) and then match the solutions at the border of each of the two bodies. This is similar, but not identical to the standard method of analysis of these models (see Appendix E).

Now prior to tackling the two body problem for the chameleon field, it is crucial to review some of the main relevant aspects of the one body problem, i.e., the situation where the *test* body does not back react on the scalar-field configuration, because some of those approximations will be used in the treatment of the two body problem. However, in our approach, it is essential that the back reaction of the field to the presence of the two bodies, be fully taken into account.

Let us consider a spherically-symmetric and *homogeneous* body of radius R and density ρ_{in} immersed in an external medium of density ρ_{out}. We will call this body, the *larger body*, as opposed to the *smaller body* that will be introduced later. The corresponding EMT's, $T_{\text{in(out)}}^m$ are assumed to be of a perfect fluid: $T_{\text{in(out)}}^m = -\rho_{\text{in(out)}} + 3P_{\text{in(out)}}$, where the scripts in(out) will refer to the interior (exterior) of the body, respectively. In this case we will consider two regions (interior and exterior), and since $P \ll \rho$ for non-relativistic matter, we neglect the pressure. Consequently,

$$\rho = \begin{cases} \rho_{\text{in}} & r \leq R \\ \\ \rho_{\text{out}} & r > R \end{cases}, \tag{8}$$

where R is the radius of the body.

In order to solve the chameleon equation Eq.(6) with the effective potential (7) we can adopt several possible strategies. Clearly, one consists in solving numerically the full non-linear chameleon equation without any approximation. In the case of a one body problem in spherical symmetry (where the test body does not backreact on the chameleon field), the chameleon equation becomes an ordinary differential equation and it can be solved using a Runge-Kutta scheme. Indeed, this was done by Khoury & Weltman [1] in their pioneering paper, in order to check the analytical

solution for the one body problem. Besides, Elder et al [41] and Schlogel et al [40], also solved numerically the chameleon equation to study atomic interferometry experiments. For this experimental situation, the test body is of the size of an atom, and therefore it is appropriate to calculate the force using the one body problem solution.

However, in the two-body problem where the test body is considered not as a point particle but as an extended body which backreacts on the chameleon field, solving the full non-linear chameleon equation entails to solving a very complicated partial differential elliptic equation. In order to advance in this direction, we postpone this analysis for the future, and consider to solve a linear elliptic equation by approximating the effective potential. To this end, there are two possible approximations. These depend actually on the specific setup, like the size of the bodies, their density, the environment's density, and the actual value of the coupling β. The values of these parameters determine, for example, if the bodies have or not a *thin shell* or even an intermediate situation where the *shell* is not *thin* nor *thick*. The thin (thick) shell dimensionless parameter $\frac{\Delta R}{R}$ (cf. Section E) allows us to determine in which regime the large or the test body is. Namely, if $\Delta R/R \ll 1$ the body has a thin shell, whereas $1 \lesssim \Delta R/R$ corresponds to a thick shell regime. Thus, depending on each of the two regimes one can approximate differently the effective potential.

If the *thin shell* condition is satisfied, the expansion of the effective potential $V_{\text{eff}}(\varphi)$ about its minimum up to the quadratic terms, for each one of the regions, as all higher order terms are ignored provides a good approximation for the determination of the scalar field profile (see for example, [1, 20, 21, 24]). Such approximation leads to a linear differential equation for the chameleon field. In a forthcoming paper we plan to study in detail the corrections to this approximation arising from higher order terms [31]. We will see that the corrections become relevant for $n > 4$ [31][5]. Next, we will describe the *quadratic approximation* to the effective potential and at the end of this subsection, we will discuss if it is appropriate for the experimental situations at hand .

We now proceed to deal with the simple, one body problem, taken to be immersed within a single medium acting as the environment. In section IIB, we generalize this expansion for the "two body problem".

The expansion of the effective potential about the corresponding minimum in each region up to the quadratic term gives:

$$V_{\text{eff}}^{\text{in,out}}(\varphi) \simeq V_{\text{eff}}^{\text{in,out}}(\varphi_{\text{min}}^{\text{in,out}}) + \frac{1}{2}\partial_{\varphi\varphi}V_{\text{eff}}^{\text{in,out}}(\varphi_{\text{min}}^{\text{in,out}})[\varphi - \varphi_{\text{min}}^{\text{in,out}}]^2, \tag{9}$$

The effective mass of the chameleon is then defined in the usual way:

$$m_{\text{eff}}^{2\text{in,out}}(\varphi_{\text{min}}^{\text{in,out}}, \beta_i, T_{\text{in,out}}^m) = \partial_{\varphi\varphi}V_{\text{eff}}^{\text{in,out}}(\varphi_{\text{min}}^{\text{in,out}}). \tag{10}$$

In particular, setting $\beta_i = \beta$, the expression for the effective mass $m_{\text{eff}}^{\text{in,out}}$ turns out to be:

$$m_{\text{eff}}^{2\text{in,out}}(\varphi_{\text{min}}^{\text{in,out}}, \beta, T_{\text{in,out}}^m) = \lambda n(n+1)M^2\Big(\frac{M}{\varphi_{\text{min}}^{\text{in,out}}}\Big)^{n+2}, \tag{11}$$

with

$$\varphi_{\text{min}}^{\text{in,out}} = M\Big(\frac{n\lambda M_{pl}M^3}{-\beta T_{\text{in,out}}^m}\Big)^{\frac{1}{n+1}}. \tag{12}$$

Expressions (11) and (12) are valid when n is a positive integer or a negative even integer, as otherwise a minimum does not exist. Furthermore, for $n = -2$ the effective mass does not depend on the composition of the body or the environment.

Now, let us consider the interesting situation where we have two bodies, the large one and the test body. The effective potential must be expended in various regions: the interiors of the two bodies and their exterior which is associated with the environment. Typically the density of the large body is much larger than the density of the environment ($\rho_{\text{out}} \ll \rho_{\text{in}}$), thus taking $T \sim -\rho$ leads to $\varphi_{\text{in}}^{\text{min}} \ll \varphi_{\text{out}}^{\text{min}}$. The effective potential inside the large body develops a minimum $V_{\text{eff},\text{in}}^{\text{min}}$ at $\varphi_{\text{in}}^{\text{min}}$ which is much larger than the minimum of the effective potential $V_{\text{eff},\text{out}}^{\text{min}}$ at $\varphi_{\text{out}}^{\text{min}}$ associated with the environment (see Fig. 1). The difference between the $\varphi_{\text{in}}^{\text{min}}$ and $\varphi_{\text{out}}^{\text{min}}$, which can be very large, depends on the density of the materials involved and the value of model's parameters. This, in turn, can lead to different types of approximations used to describe V_{eff}. For instance, since we take the environment to extend to infinity, the chameleon field must be such that it reaches $\varphi_{\text{out}}^{\text{min}}$ at spatial infinity. Therefore the field must interpolate between $\varphi_{\text{out}}^{\text{min}}$ at spatial infinity and φ_{in}^c at the centers of the each of the two bodies, both modelled as spherical (see
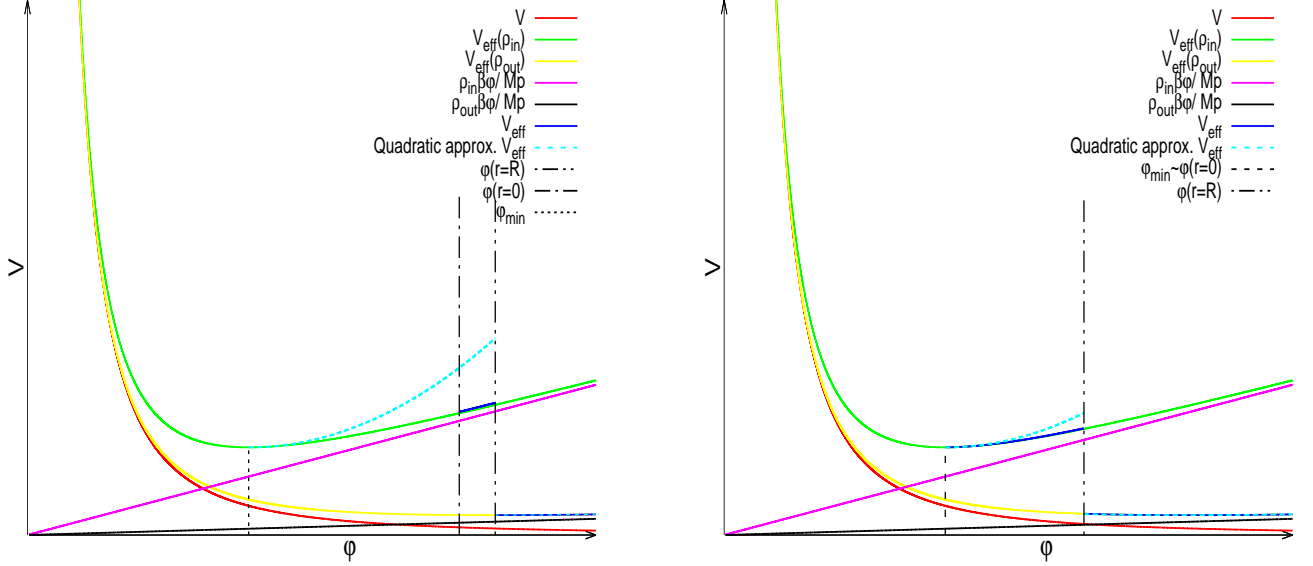

Figure 1: Effective potential inside and outside the large body. The blue line shows the potential $V_{\text{eff}}(\varphi)$ for the one body problem, the red line shows $V_{\text{eff}}(\varphi)$ for $\rho = \rho_{\text{out}}$ in Eq.7, the green line shows $V_{\text{eff}}(\varphi)$ for $\rho = \rho_{\text{in}}$ in Eq.7 and the light blue line shows the quadratic approximation Left: The *thick shell* case; Right: The *thin shell* case.

Figure 2). We emphasize that this central values need not coincide with $\varphi_{\text{in}}^{\text{min}}$ the actual minima of the function $V_{\text{eff}}^{\text{in}}(\varphi)$ in the bodies' interior. Now, roughly speaking the chameleon field rolls up the potential $V_{\text{eff}}^{\text{out}}$ from its minimum at $\varphi_{\text{out}}^{\text{min}}$ to the value φ_R where the field reaches the surface of the large body (respectively, the test body), where R stands schematically for the location of the border of the body. However, and this is an essential aspect of the present analysis, the field configuration is not really constant and it is precisely the resulting directional dependence that is associated with a non-vanishing force (in the direction of the large body) on the test body.

Now, when $\varphi_R \sim \varphi_{\text{out}}^{\text{min}}$ we can rely on the quadratic expansion about its minimum as a good approximation to $V_{\text{eff}}^{\text{out}}$ since the field outside the bodies takes values that are always close to the minimum $V_{\text{eff},\text{out}}^{\text{min}}$. We report results only for those situations where the energy criterion favors our approximations over that of the standard approach. Now, at the border of the bodies, the effective potential experiences a discontinuous jump (due to the jump between the body's and the environment's densities) and at φ_R we have to use an approximate expression for $V_{\text{eff}}^{\text{in}}$ instead of one for $V_{\text{eff}}^{\text{out}}$ in order to solve the chameleon equation inside the body. However, as is standard in these cases, the field itself φ (together with its first derivative) must be continuous everywhere, and in particular at the surface of the bodies. As one moves towards the interior of the bodies, the field φ starts to "roll down" the potential $V_{\text{eff}}^{\text{in}}$ towards its minimum, but without necessarily reaching it. More specifically, the field configuration interpolates from its surface value and the value φ_{in}^c at the center of the body. If $\varphi_R \sim \varphi_{\text{in}}^c \sim \varphi_{\text{in}}^{\text{min}}$, it means that the field is already near the minimum of the potential inside the body and the quadratic expansion about the minima is a very good one. This situation is emblematic of a *thin shell* regime. On the other hand, when $\varphi_{\text{in}}^{\text{min}} \sim \varphi_{\text{in}}^c \ll \varphi_R$, we have a situation where the field at the body's surface is very far from its minima, and thus, the *quadratic* approximation for $V_{\text{eff}}^{\text{in}}$ is not necessarily a very good one. In that case, however, $V_{\text{eff}}^{\text{in}}$ is usually dominated by the matter dependent part, and then one may use the approximation $V_{\text{eff}}^{\text{in}} \sim \rho_{\text{in}} \frac{\beta\varphi}{M_{pl}}$ [1]. This happens in some situations in which the large body falls within the *thick shell regime*; as for the example the Sun with $n = 1$, $M = 10$ eV and $\beta \ll 1$.

In the present paper we shall focus mainly in scenarios where the bodies are within *thin shell regime*, and thus, where the quadratic approximation to the effective potential is adequate. In Section III we shall develop a criteria to assess the extent to which this approximation is in fact a good one using a minimization of a suitable energy functional.
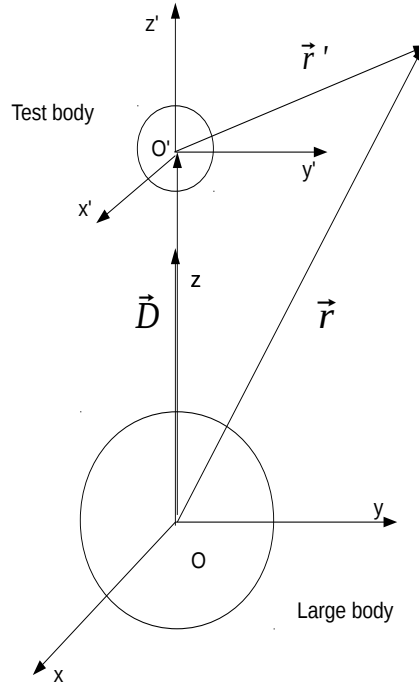
Figure 2: Two body problem.

B.   The two body problem

We proceed with the calculation of the chameleon in the presence of two bodies without, in principle, neglecting any contribution, but still within the *quadratic* approximation for the effective potential discussed before. The geometry of the problem is depicted in Fig. 2.

In order to do so, we expand the most general solution in complete sets of solutions of the differential equation in the inside and outside regions determined by the two bodies. Thus we write,

$$\varphi = \begin{cases} \varphi_{\text{in1}} = \sum\limits_{lm} C_{lm}^{\text{in1}} i_l(\mu_1 r) Y_{lm}(\theta,\phi) + \phi_{1\text{min}}^{\text{in}} & (r \leq R_1) \\ \varphi_{\text{out}} = \sum\limits_{lm} C_{lm}^{\text{out1}} k_l(\mu_{\text{out}} r) Y_{lm}(\theta,\phi) + C_{lm}^{\text{out2}} k_l(\mu_{\text{out}} r') Y_{lm}(\theta',\phi') + \varphi_\infty & (\text{exterior solution}) \\ \varphi_{\text{in2}} = \sum\limits_{lm} C_{lm}^{\text{in2}} i_l(\mu_2 r') Y_{lm}(\theta',\phi') + \varphi_{2\text{min}}^{\text{in}} & (r' \leq R_2) \end{cases} \tag{13}$$

where $\mu_1 = m_{\text{eff}}^{\text{large body}}$, $\mu_{\text{out}} = m_{\text{eff}}^{\text{out}}$, $\mu_2 = m_{\text{eff}}^{\text{test body}}$ and R_1, R_2 are the radii of the *large* and *test* bodies, respectively, and i_l and k_l are Modified Spherical Bessel Functions (MSBF). In the above equation, the Cartesian coordinate system x,y,z is centered in the *large* body, while the coordinate system x',y',z' is centered in the *test* body (see Fig. 2). Notice that in writing Eq. (13) we have taken into account the regularity conditions of the scalar field at the center of both bodies. That is, the MSBF used in the expansions for the solutions inside both bodies are well behaved within their corresponding compact supports. Conversely, for the exterior solution (i.e. the solution outside both bodies) we employ the set of MSBF functions associated with each body which are well behaved at infinity. Furthermore, the coefficients C_{lm} of Eq. (13) are calculated using the following continuity conditions for the field and its derivative at the boundaries of the two bodies:

$$\varphi_{\text{in1}}(r = R_1) = \varphi_{\text{out}}(r = R_1), \qquad \partial_r \varphi_{\text{in1}}(r = R_1) = \partial_r \varphi_{\text{out}}(r = R_1),$$

$$\varphi_{\text{in2}}(r' = R_2) = \varphi_{\text{out}}(r' = R_2), \qquad \partial_{r'} \varphi_{\text{in2}}(r' = R_2) = \partial_{r'} \varphi_{\text{out}}(r' = R_2);$$

In order to describe properly the two body problem in a single coordinate system we can use the following relationship
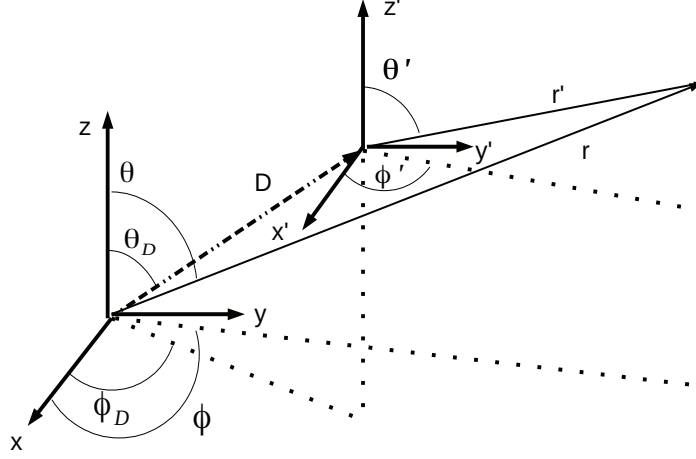
Figure 3: Coordinates transformation.

(see Figure 3) that links the special functions in the two coordinate systems [32, 33]:

$$k_l(\mu_{\text{out}}r)Y_{lm}(\theta,\phi) = \sum_{vw} \alpha^{*lm}_{vw} i_v(\mu_{\text{out}}r')Y_{vw}(\theta',\phi'), \tag{14}$$

where the coefficients α^{*lm}_{vw} can be expressed as follows:

$$\alpha^{*lm}_{vw} = (-1)^{m+v}(2v+1) \sum_{p=|l-v|}^{|l+v|} (-1)^{-p}(2p+1) \left[\frac{(l+m)!(v+w)!(p-m-w)!}{(l-m)!(v-w)!(p+m+w)!} \right]^{1/2}$$
$$\times \begin{bmatrix} l & v & p \\ 0 & 0 & 0 \end{bmatrix} \begin{bmatrix} l & v & p \\ m & w & -m-w \end{bmatrix} k_p(\mu_{\text{out}}|D|)Y_{p(m-w)}(\theta_D,\phi_D), \tag{15}$$

being θ_D and ϕ_D the angular coordinates associated with the vector $\vec{D}$ (see Fig. 3) and we remind the reader that D is the distance between the center of the two bodies.

Moreover, we can use a similar relationship between the special functions given in terms of the coordinates centered in the *test* body with the ones centered in the *large* body:

$$k_l(\mu_{\text{out}}r')Y_{lm}(\theta',\phi') = \sum_{vw} \alpha^{lm}_{vw} i_v(\mu_{\text{out}}r)Y_{vw}(\theta,\phi), \tag{16}$$

where

$$\alpha^{lm}_{vw} = (-1)^{m+v}(2v+1) \sum_{p=|l-v|}^{|l+v|} (2p+1) \left[\frac{(l+m)!(v+w)!(p-m-w)!}{(l-m)!(v-w)!(p+m+w)!} \right]^{1/2}$$
$$\times \begin{bmatrix} l & v & p \\ 0 & 0 & 0 \end{bmatrix} \begin{bmatrix} l & v & p \\ m & w & -m-w \end{bmatrix} k_p(\mu_{\text{out}}|D|)Y_{p(m-w)}(\theta_D,\phi_D), \tag{17}$$

valid for $|r| \le |D|$ and $|r'| \le |D|$. We make use of the axial symmetry of the problem and thus set the $z-$axis as containing the centers of the two bodies (see Fig.2). Thus, the coordinate transformation is, in this case, a translation along this axis. Therefore, $\theta_D = 0$ and φ_D becomes irrelevant do to the axial symmetry. An approximate expression for the chameleon field is found by truncating the infinite series Eqs. (14) and (16). We further note that as shown in Refs.[34, 35], the series of this type can be estimated by truncating the sum after the first N terms, with N given by the integer part of $N_0 = \frac{e\mu_{\text{out}}|D|}{2}$ where e is Euler's number. Using this last result we can solve the following two equations for C_l^{out1} and C_l^{out2}; the first one reads:

$$b_1\delta_{l0} = C_l^{\text{out1}}a_l + \sum_{w=0}^{N} C_w^{\text{out2}}z_{wl}, \tag{18}$$

where

$$a_l = \frac{k_l'(\mu_{\text{out}}R_1)i_l(\mu_1 R_1)}{i_l'(\mu_1 R_1)} - k_l(\mu_{\text{out}}R_1), \tag{19}$$

$$z_{wl} = \alpha_{l0}^{w0}\left[i_l(\mu_{\text{out}}R_1) - \frac{i_l'(\mu_{\text{out}}R_1)i_l(\mu_1 R_1)}{i_l'(\mu_1 R_1)}\right], \tag{20}$$

$$b_1 = \sqrt{4\pi}(\varphi_\infty - \varphi_{1\text{min}}^{\text{in}}). \tag{21}$$

where a *prime* ''' indicates differentiation of the MSBF with respect to its argument.

The second equation reads:

$$b_2\delta_{l0} = C_l^{\text{out2}}x_l + \sum_{w=0}^{N} C_w^{\text{out1}}y_{wl}, \tag{22}$$

where

$$x_l = \frac{k_l'(\mu_{\text{out}}R_2)i_l(\mu_2 R_2)}{i_l'(\mu_2 R_2)} - k_l(\mu_{\text{out}}R_2), \tag{23}$$

$$y_{wl} = \alpha_{l0}^{*w0}\left[i_l(\mu_{\text{out}}R_2) - \frac{i_l'(\mu_{\text{out}}R_2)i_l(\mu_2 R_2)}{i_l'(\mu_2 R_2)}\right], \tag{24}$$

$$b_2 = \sqrt{4\pi}(\varphi_\infty - \varphi_{2\text{min}}^{\text{in}}). \tag{25}$$

We can now write the system of equations for the coefficients C_l^{in1} and C_l^{in2} associated with the interior solutions in terms of the coefficients of the exterior solution:

$$C_l^{\text{in1}}i_l'(\mu_1 R_1) = C_l^{\text{out1}}k_l'(\mu_{\text{out}}R_1) + \sum_{w=0}^{N} C_w^{\text{out2}}\alpha_{l0}^{w0}i_l'(\mu_{\text{out}}R_1), \tag{26}$$

$$C_l^{\text{in2}}i_l'(\mu_2 R_2) = C_l^{\text{out2}}k_l'(\mu_{\text{out}}R_2) + \sum_{w=0}^{N} C_w^{\text{out1}}\alpha_{l0}^{*w0}i_l'(\mu_{\text{out}}R_2). \tag{27}$$

In this way, by solving the system of equations (18) and (22) we can obtain a solution of the two body problem for the chameleon where we perform an approximation (within the quadratic approach of the effective potential) consisting in the truncation of the series used for the transformation of coordinates. The dependence of the field on the composition of the *test* body appears through the constants C_l^{out1} and C_l^{out2}.

Figure 4 depicts the field around the centers of the two bodies and outside them along the $z-$axis which results from our method by cutting off the series expansions after taking the first three terms in each one[6]. We also show, for comparison, the field obtained by Khoury & Weltman [1] using the analytical solution to the linearized time-independent chameleon field equation for one body (we will refer to this solution as that of the standard approach)[7]. Note that under the conditions $1 \ll \mu_{1,2}R_{1,2}$, which are valid within each body, the *thin shell* effect appears in both bodies. Namely, the field is almost constant with values close to $\varphi_{\text{min}\,1,2}$ in each body, respectively, and grows exponentially near the surfaces. As μR becomes smaller, the *thin shell* disappears. Moreover, Figure 4 (right panel) compares the chameleon field obtained within the framework of the standard approach with the corresponding field obtained with our two-body method in the region where the *test* body is located. In order to check our method, we compute the solution for the one body problem using our approach, and verify that we recover the same results as in Ref. [1].

---

[6] The same result is obtained if only the first term of the series is used as this turns out to be many orders of magnitude larger than the following terms.

[7] We have verified that this solution agrees to a very good approximation with the numerical solution to the non-linear chameleon field equation for one body.
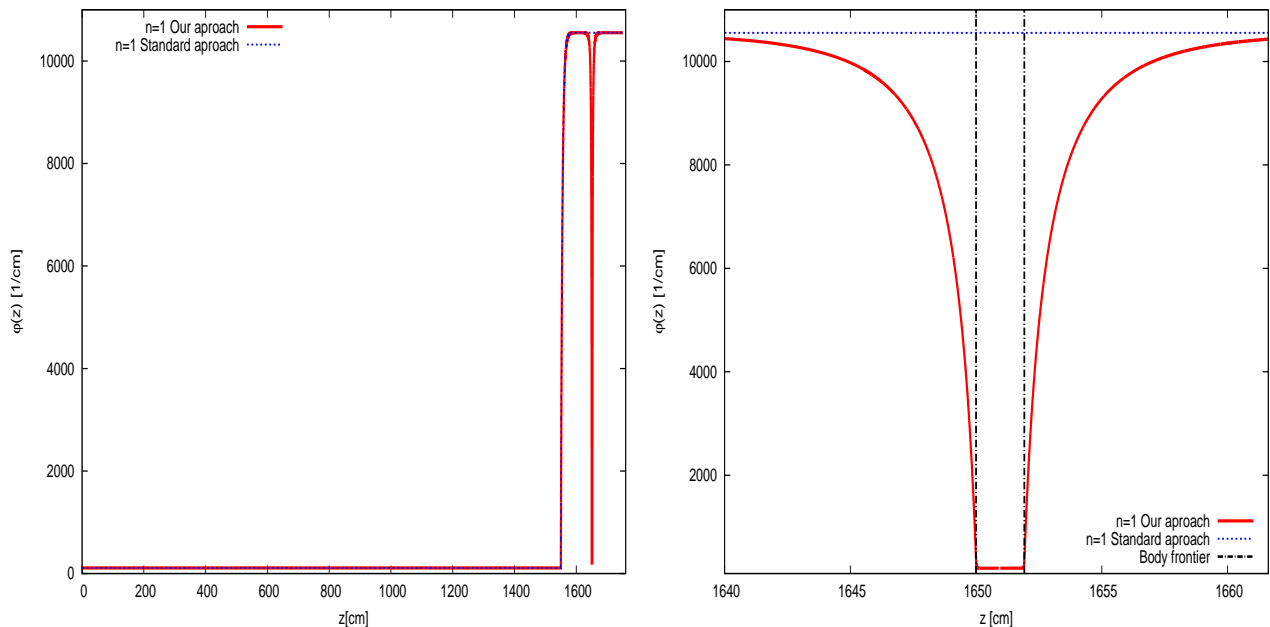
(a) Chameleon field within a neighbourhood of the *large* body.   (b) Chameleon field within a neighbourhood of the *test* body.

Figure 4: The chameleon field φ as a function of coordinate z inside the bodies and in their outskirts (z is the distance to the center of the *large* body in cm, then φ is measured in cm^{-1}). The *large* body consists of a sphere of radius $R_1 = 1550$ cm and $\mu_1 = 197.2244$ cm^{-1}. This body mimics roughly the actual hill where the experiment of the Eöt-Wash group takes place and which produces the desired combined effects (gravitational and "fifth" force if any). The *test* body consists of a 10 gr sphere of aluminium and has a radius $R_2 = 0.96$ cm and $\mu_2 = 78.1940$ cm^{-1} . In both figures $n = 1 = \beta = 1$ and $M = 2.4$ meV and $\rho_{out} = \rho_{\mathrm{atm}} = 10^{-3}$ g cm^{-3} Red line: Our approach, Blue Line: Standard Approach [1].

III. MINIMUM ENERGY CRITERION

It is well known that the classical solution of a field equation corresponds to an extreme of the action (with fixed boundary conditions). When we are interested in static solutions, such extreme coincides with the field configuration that minimizes the energy functional. That well known result is used in this section to construct an appropriate energy functional $U[\varphi, \rho, \beta]$ associated with the class of test field configurations which can be used to compare the quality of various approximations to the true solution of the differential equation satisfied by the scalar field. This will empower us to determine based on an objective quantitative criteria when our analysis should be trusted over other treatments and when the opposite is true. In the next section, we obtain the chameleon mediated force from the variation with distance of this functional.

A first naive attempt to find $U[\varphi, \rho, \beta]$ consists in considering the time-time component of the energy-momentum tensor associated with the system, which in turn, is the source of the Einstein's field equations of the model. Thus, we focus on the gravitational field equations that are obtained from varying the action (1) with respect to $g^{\mu\nu}$: [8]

---

[8] From the Bianchi identities followed by the use of Eq. (6) one can see that the EMT of matter is not conserved in the Einstein frame: $\nabla^\mu T^m_{\mu\nu} = T^m(\partial_\varphi \ln A)\nabla_\nu\varphi$, where $A^2 = e^{2\beta\varphi/M_{pl}}$ is the conformal factor between the Einstein-frame metric and the geodesic metrics [cf. Eq. (2)]. We then obtain $\nabla^\mu T^m_{\mu\nu} = T^m\beta/M_{pl}\nabla_\nu\varphi$. The right-hand side of this equation is precisely related with the chameleon force [cf. Eq. (B8)].

$$G_{\mu\nu} \;=\; \frac{1}{M_{pl}^2}\left(T_{\mu\nu}^{\varphi} + T_{\mu\nu}^{m}\right) \;, \tag{28}$$

$$T_{\mu\nu}^{\varphi} \;=\; (\nabla_\mu\varphi)(\nabla_\nu\varphi) - g_{\mu\nu}\left[\frac{1}{2}g^{\alpha\beta}(\nabla_\alpha\varphi)(\nabla_\beta\varphi) + V(\varphi)\right] \;, \tag{29}$$

where, as before, we assume $T_{\mu\nu}^{m} = u_\mu u_\nu(\rho + P) + g_{\mu\nu}P$ for the EMT of matter. Now the energy associated with the total EMT under the assumptions of staticity and flat space-time is

$$U \;=\; \int_V (T_{00}^{\varphi} + T_{00}^{m})\,dV = \int_V \left[\frac{1}{2}(\nabla^i\varphi)(\nabla_i\varphi) + V(\varphi) + \rho\right] dV \;, \tag{30}$$

where the time components of both EMT's are taken with respect to an observer that is static relative to the two-body configuration [9].

While this energy functional certainly contains the total energy of the system from the Einstein-frame point of view, the extremization of this functional with respect to φ with fixed densities (i.e., as considered independent of φ) does not lead to the static chameleon equation that is obtained from Eq.(6). That is, we require an energy functional extremized by the actual field configuration. As a consequence we turn our attention to the more appealing functional given by

$$U_{\rm eff} \;=\; \int_V \left[\frac{1}{2}(\nabla^i\varphi)(\nabla_i\varphi) + V_{\rm eff}(\varphi)\right] dV \;, \tag{31}$$

where the integral is computed over the whole Euclidean three-dimensional space (i.e. $\mathbb{R}^3$) and where the effective potential $V_{\rm eff}(\varphi)$ at each point of space is the one corresponding to the density of matter at that point (associated with each of the bodies and the media respectively) and which is given by (7).

We can rewrite the functional (31) integrating by parts , which leads to

$$U_{\rm eff} = \int_V \left[-\frac{1}{2}\varphi\nabla^2\varphi + V_{\rm eff}(\varphi)\right] dV \;, \tag{32}$$

where we discarded the irrelevant surface term which must vanish at infinity.

One issue that is extremely important to have in mind is the fact that the validity of our analysis does depend on the accuracy of approximation used in the expansion of the effective potential for the scalar field in each region of space. In the present work, as we have explained earlier, we have used quadratic expansions around the minimum of the effective potential in each one of the regions involved. This should clearly be a very good approximation when all the bodies involved (including the media between the solid bodies) are in the so called deep *thin shell* regime. However, that regime is only identified heuristically, and sharp boundaries delimiting the exact regions in parameter space simply do not exist, and in fact should not exist as the transition between *thin* and *thick* shell regimes must undoubtedly be a smooth one. This faces us with a problem when trying to establish when our results are more trustworthy that the existing ones. The problem would of course be resolved if one had exact solutions for the complete specific problem at hand, involving all the bodies present in the actual experimental situation, or one that included at least the most relevant ones, namely the source body, the test body, and the media in between them. We note that the relatively simple treatments that consider exact solutions for just one body surrounded by a media and then use the gradient of the resulting scalar field at the location of the second body while ignoring the effect of such body on the field itself, and then attempt to correct for the so called *thin shell* effect by introducing a simple multiplicative factor extracted from consideration of another one body problem, cannot be considered *a priori* more reliable than our method. However, we must recognize, of course, that it is possible that under some circumstances, those analyses might provide better estimates than ours. That would of course correspond to situations where our second order expansion fails to provide an accurate enough characterization of the potential in the regime explored by the actual scalar field configuration. That can lead to situations where it is not clear which results should one trust.

---

[9] That is, we take a reference frame defined by the unit time-like vector (4-velocity) $n^\mu = \left(\frac{\partial}{\partial t}\right)^\mu$ as to coincide with u^μ, such that $T_{00}^{\rm tot} = n^\mu n^\mu T_{\mu\nu}^{\rm tot}$, where $T_{\mu\nu}^{\rm tot} = T_{\mu\nu}^{\varphi} + T_{\mu\nu}^{m}$. The staticity assumption translates into $n^\mu\partial_\mu\varphi = 0$.

Fortunately there is a simple method to discriminate between two approximated solutions to the static field configuration corresponding to a given distribution of sources and media. We refer here to the fact that the field configuration corresponding to the solution is an extreme of the action functional which, for static situations, correspond to the minima of the energy functional. The point is then that when faced with two approximations to a given problem one can determine which one is a better approximation by comparing the value of the energy functional of the two configurations. Of course in making this comparison it is essential that one uses the same energy functional and fixes the relevant bodies and interpolating media to be exactly the same when making the energetic comparison. The configuration with the lowest value of the energy functional provides a better approximation and thus should be better trusted. Of course ideally one would prefer an exact solution but lacking that, we must rely on the better one of the approximations.

We have carried out precisely such analysis in order to compare the field configurations emerging from our analysis with the field configurations obtained by Khoury & Weltman [1]. As mentioned above, the relevant energy functional is given by Eq.(32). We note by looking at this equation that the second term of the integrand will contain a constant corresponding to the minimum of the effective potential which is determined by the environment. This constant does not affect the calculation of the chameleon force between the bodies because the force is derived from the variation of the potential U_{eff} with respect to the bodies' separation and the contribution from such a constant, as long as the bodies are not deformed, is independent of the separation. On the other, the integral of such constant in the whole space, extending to infinity, would lead to an infinite contribution for the energy. In any event it is clear that such term is irrelevant in the determination of the force between two bodies [10]. In view of this, and in order to work with only finite energy functionals, we proceed to "renormalize" our expressions by subtracting the divergent term, and considering just,

$$U_{\text{eff}}^* = \int_V \left[-\frac{1}{2}\varphi\nabla^2\varphi + V_{\text{eff}}(\varphi) - V_{\text{eff}}(\varphi_{\text{min}}^{\text{out}}) \right] dV \ . \tag{33}$$

In this paper, we analyse two experimental situations: i) the Eöt-Wash torsion balance: an Earth based experiment where the large body is a mountain and the test bodies are centimeter-size metal sphere and ii) the Lunar Laser Ranging experiment where the large body is represented by the Sun and the test bodies by the Earth and the Moon. In each scenario the bodies are surrounded by an environment, which is described in more detail in Sections V A and V B.

For each of the experimental situations considered in detail in this work we have computed the value of the above functional Eq.(33) corresponding to the two body problem using the field configuration obtained with our method (described in Section II B) and that corresponding to the field configuration obtained in the standard approach. We remind the reader that in such approach (as exemplified by the work of Khoury and Weltman) the effect of the small body is ignored when determining the scalar field configuration, and the force on the latter is estimated by simply considering the gradient of the field corresponding to the large body and the environment at the location of the small body (see Appendix B) with some additional factors which are related with the thin shell parameter $\Delta R/R$. Moreover it often relies on a approximated expression for the effective potential that differs from that the one we employ (see Appendix E).[11] On the other hand, a solution considering the contribution of the test body was proposed by Hui et al [21] and used in Refs. [22, 43] to calculate the Eötvös parameter. In that work, a superposition of the one body problem solution of both the *large* and the *test* bodies is considered. Furthermore, the authors claim that this solution is valid outside both bodies. However, no expression for the field inside the bodies is provided. Therefore, it is not possible to apply the energy criterion proposed in this section to the above mentioned solution [12]. The values of η shown in Section V are computed from Eqs. 41a and 41b. However the reader should take into account that using such expressions for η within the Khoury and Weltmann approach yields strictly speaking $\eta = 0$ for universal β given the fact that in such analysis the test body is treated as a point particle.

Figure 5 shows the results for the Eöt-Wash torsion balance. The test body (Al) and the source (the mountain) are taken as immersed in the same environment when computing the energy of the field configurations. We considered

---

[10] In the realistic context of the full fledge chameleon theory that term would have to be regarded as a contribution to the "cosmological constant".

[11] As regards the expressions obtained by Mota & Shaw [19] for the chameleon field, we could not apply the energy criterion since the explicit expression for the chameleon field is not reported in their work but they just present an expression of the derived force.

[12] Nevertheless, we applied the energy criterion to the region where the field is defined and found that our solution has lower value of the energy functional

the cases $M = 2.4$ meV (the cosmological chameleon) with ρ_{out} as the density of the vacuum-chamber while for the case $M = 10$ eV, ρ_{out} was taken as the atmosphere's density. For the case $M = 2.4$ meV (left panel) the relative difference of the energy functional is small but the energy of the field configuration obtained with our method is always smaller. We have also checked that similar results are obtained for various values of n. On the other hand, for the case $M = 10$ eV, the situation is different. Figure 5 (right panel) shows that for $n = 1$ and $\beta < 10$ the energy criterion indicates that our approach yields an energy that is much larger than the corresponding energy obtained in the standard approach which indicates that the latter is much trustworthy. On the other hand, for $\beta > 10$ the two body problem with the *quadratic* approximation for V_{eff} is a better solution to the exact problem than the one obtained from the standard approach[13]. It should be noted, that we could not apply our energy criterion to the most realistic case where one includes the metal shell of the vacuum chamber in the modeling for the Eötvös torsion balance experiment. This is because we cannot compare with the standard approach since, as far as we are aware, it does not usually include the explicit determination of the chameleon field's profile corresponding to this aspect of the experimental device. [14] [15]. Figure 6 compares the values of the energy functional computed for the LLR experiment obtained from our method and from the standard approach taking $M = 10$ eV. The density of the environment is assumed to be the one of the interstellar medium $\rho_{out} = 10^{-24}$g cm^{-3} and the vertical dotted lines show the onset of the thin shell condition for Earth and Sun respectively (for values of β lower than the corresponding to vertical lines, the thin shell condition does not hold). For the cosmological chameleon, the energy criterion indicates that our solution is a better approximation than the one obtained in standard approach for $n = 1, 2, 3, 4$ and for the values of β considered here [16]. Moreover, for $M = 10$ eV we find that for each of the tested values of n, there is a region (which corresponds to the case where the large body satisfies the *thin* shell condition, while the *test* body may not) where the energy criterion indicates that the field profile obtained by our method is a better solution than the one obtained in the standard approach. On the other hand, for the β values excluded from that region (this is the case where the large body fails to satisfy the *thin shell* condition), the KW approach gives a better result (see Fig.6) .

We will limit the results of this paper to the case where the *quadratic* approximation to the effective potential is a good one and leave for a future work [26] the case where another approximation has to be considered. It should be stressed, that for both experimental situations there are ranges of the model's parameters for which despite the fact that the *test* body does not satisfy *thin shell* condition, the energy criterion indicates that the scalar field profile obtained by considering the full two body problem within the *quadratic* approximation for the effective potential yields a better approximation to the exact solution than the one used within the standard approach. On the other hand, when the *thin shell* condition does not hold for the *large* body, the energy criterion always indicates that the standard approach yields a better approximation than the one obtained by the method proposed in this work, i.e., indicating that it is essential to employ something like the *thick shell* approximation for the effective potential.

---

[13] For $\beta > 10^2$ the relative difference is of order 10^{-3} but always positive. This cannot be appreciated from the left panel of Figure 5 due to the scale of the plot. For each of the values of n considered here such transition takes place at a different value of β (see Table III in Section V)

[14] Ref. [25] obtains a numerical solution for the torsion pendulum which has a different geometry than the torsion balance analyzed in this paper and estimates the effect of including a shell in the value of the force. Most analyses focused in the Eötvös torsion balance do not include the metal encasing in the calculation of the field and/or the force [1, 19, 21, 22, 24].

[15] In section V A, we estimate the value of η for the standard approach including the effect of the metal shell through multiplication of a correction term as suggested by [25].

[16] For $M = 2.4$ meV (the cosmological chameleon) and the β values that we test, the *thin shell* holds always for the Sun, Earth and Moon.

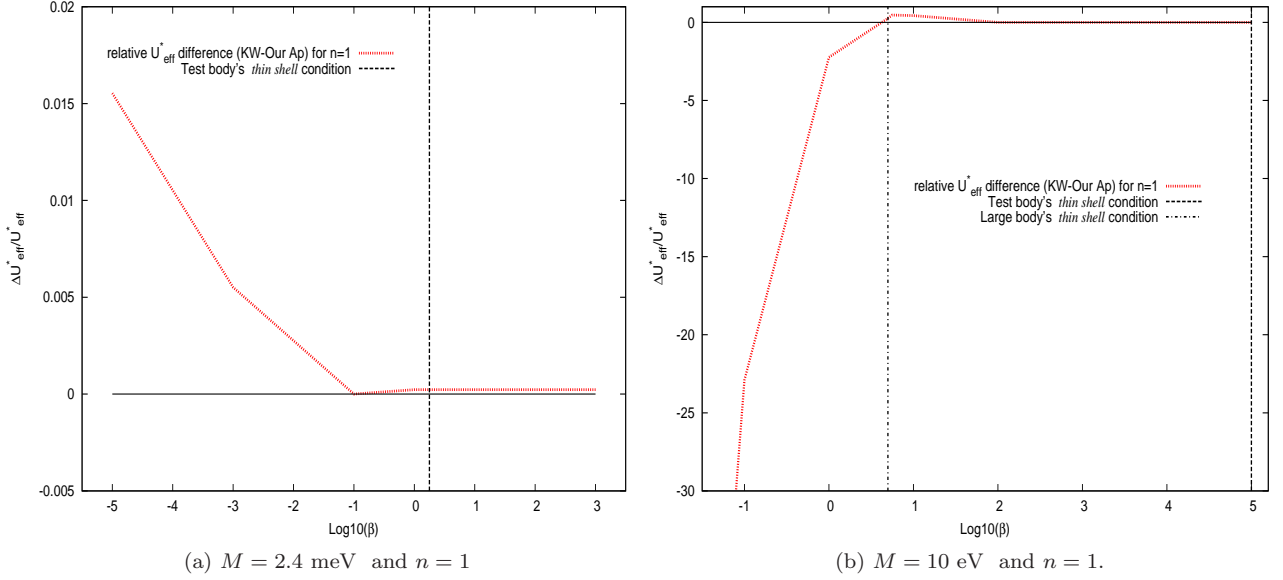(a) $M = 2.4$ meV and $n = 1$

(b) $M = 10$ eV and $n = 1$.

Figure 5: Relative difference of energy ($\frac{U_{\text{standard}} - U_{\text{our approach}}}{U_{\text{standard}}}$) computed for the Eötvös experiment. The density of the environment surrounding both the test body (Al) and the source (the mountain) is assumed to be the same. Left: $M = 2.4$ meV and $\rho_{out} = 10^{-7}$g cm^{-3} for the density of the vacuum chamber. The *thin shell* condition for the mountain is always satisfied, while for β lower than the value indicated by the vertical dotted line the *test* body does not have a thin shell. Right: $M = 10$ eV and $\rho_{out} = 10^{-3}$g cm^{-3} for the density of the atmosphere. The vertical dotted lines show the thin shell condition limits for the *test* and the large bodies (i.e. for values of β lower than those indicated by the vertical dotted lines the *thin shell* condition does not hold) .
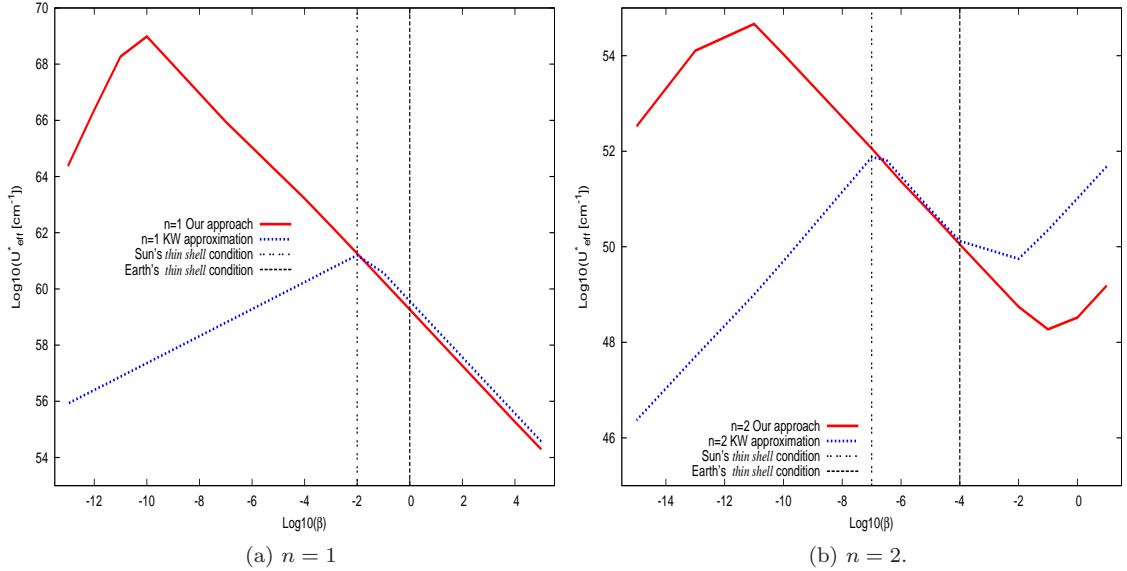

(a) $n = 1$

(b) $n = 2$.

Figure 6: Comparison of the energy computed for the LLR experiment using our approach (red) and the standard one (blue) taking $M = 10$ eV. The test body is assumed to be the Earth and the environment corresponds to the interstellar medium with density $\rho_{out} = 10^{-24}$g cm^{-3} . The vertical dotted lines show the thin shell condition for Earth and Sun (for values of β lower than those indicated by the vertical dotted lines the bodies have no thin shell).

IV.   CHAMELEON MEDIATED FORCE BETWEEN TWO SPHERICAL OBJECTS

In this section we calculate from first principles the effective chameleon force between the *large* and the *test* bodies. This force, together with the gravitational force on the *test* body, will be considered as characterizing a "free falling" *test* body in laboratory conditions under the influence of both interactions. The expression for this force together with the chameleon field computed in sections V A and V B will allow us to compute numerically the Eötvös parameter associated with the acceleration of two *test* bodies of different composition and to estimate the magnitude of the predicted violation of WEP.

As we mentioned before, the variation of the functional of Eq. (32) with respect to φ with the densities of the bodies fixed, leads to the actual equation for the chameleon for a static problem:

$$\nabla^2 \varphi = \frac{\partial V_{\text{eff}}}{\partial \varphi}, \tag{34}$$

where ∇^2 stands for the Laplacian operator in three dimensional Euclidean space.

We can rewrite the functional (31) integrating by parts and using Eq.(34), which leads to

$$U_{\text{eff}} = \int_V \left[-\frac{1}{2}\varphi\nabla^2\varphi + V_{\text{eff}}(\varphi) \right] dV = \int_V \left[-\frac{1}{2}\varphi\partial_\varphi V_{\text{eff}}(\varphi) + V_{\text{eff}}(\varphi) \right] dV \ , \tag{35}$$

where as usual, we discarded the surface term.

Using Eq,(7) we obtain after some simplifications

$$U_{\text{eff}} = \int_V \left[\frac{1}{2}V_{\text{eff}}(\varphi)(2+n) + \frac{(1+n)\beta\varphi T^m}{2M_{pl}} \right] dV \ . \tag{36}$$

At this point the energy functional is exact. However, we now use in this functional the quadratic approximation for V_{eff} about its minimum in each region of space (i.e. inside and outside the bodies).

Our goal is to work with the difference $\hat{\varphi} = \varphi - \varphi_{\min}$ rather with φ alone given that $\hat{\varphi}$ vanishes at infinity. According to this, Eq. 36 becomes,

$$U_{\text{eff}} = \int_V \left[\frac{(2+n)m_{\text{eff}}^2}{4}\hat{\varphi}^2 + \frac{(1+n)\beta T^m\hat{\varphi}}{2M_{pl}} + \frac{(1+n)\beta T^m\varphi_{\min}}{2M_{pl}} + \frac{1}{2}V_{\text{eff}}^{\min}(2+n) \right] dV \ . \tag{37}$$

The only approximation we have made so far for the energy of the whole system is to replace the effective potential of the chameleon with the corresponding expansion around its minimum in each of the three regions (i.e. the two bodies and the environment).

We can now compute the chameleon mediated force using $F_{z\varphi} = -\frac{\partial U_{\text{eff}}^{\text{trunc}}}{\partial D}$, where D is the distance between the center of the two bodies. To this aim, we first notice that the last two terms within the integral of Eq. (37) are independent of the separation D of the bodies, and thus, do not contribute to the force, i.e., $\frac{\partial}{\partial D}\{\int_V [\frac{(n+2)}{2}V_{\text{eff}}(\varphi_{\min}) + \frac{(1+n)\beta\varphi_{\min}T^m}{2M_{pl}}]dV\} = 0$ [17].

In order to calculate the total energy, we have to consider the contributions due to the chameleon in the regions inside the two bodies and in the region exterior to both bodies. To do so, let us define V_1 as the region corresponding to the *large* body, V_2 as the region corresponding to the *test* body, and V_3 is the region exterior to the *large* body in the coordinate system centered in the *large* body:

$$V_3 = \begin{cases} R_1 \leq r \leq \infty \\ 0 \leq \theta \leq \pi \\ 0 \leq \varphi \leq 2\pi \end{cases} \tag{38}$$

Thus, the relevant energy functional can be written as:

$$\begin{aligned} U_{\text{eff}} &= \int_{\text{large body}} t_{00}[\hat{\varphi}(V_1)]dV_1 + \int_{\text{test body}} t_{00}[\hat{\varphi}(V_2)]dV_2 + \int_{\text{outside bodies}} t_{00}[\hat{\varphi}(\text{out})]dV_{out} \\ &= \int_{V_1} t_{00}[\hat{\varphi}(V_1)]dV_1 + \int_{V_2} t_{00}[\hat{\varphi}(V_2)]dV_2 + \int_{V_3} t_{00}[\hat{\varphi}(\text{out})]dV_3 - \int_{V_2} t_{00}[\hat{\varphi}(\text{out})]dV_2 \end{aligned} \tag{39}$$

---

[17] As usual, the integral $\int_V V_{\text{eff}}(\varphi_{\min})dV$ (in all the space) is an infinite constant.

where $t_{00} = \frac{(2+n)}{4} m_{\rm eff}^2 \hat{\varphi}^2 + \frac{(1+n)\beta\hat{\varphi}T^m}{2M_{pl}}$ corresponds to the first two terms of Eq. (37) which are the responsible for the force between the two bodies. Here $\hat{\varphi}({\rm out})$ refers to the field outside the two bodies, and because of this definition and the arrangement of the integrals, we have to subtract the last term. In consequence, the total force can be expressed as:

$$
\begin{aligned}
F_{z\varphi} &= \frac{\partial}{\partial D} \int_{V_2} \left\{ \hat{\varphi}_{\rm in2}(\vec{r}\,') \left[\frac{(n+1)}{2} \frac{\rho_2 \beta}{M_{pl}} \right] - \frac{(2+n)\mu_2^2 \hat{\varphi}_{\rm in2}^2(\vec{r}\,')}{4} \right\} d^3\vec{r}\,' \\
&+ \frac{\partial}{\partial D} \int_{V_1} \left\{ \hat{\varphi}_{\rm in1}(\vec{r}) \left[\frac{(n+1)}{2} \frac{\rho_1 \beta}{M_{pl}} \right] - \frac{(2+n)\mu_1^2 \hat{\varphi}_{\rm in1}^2(\vec{r})}{4} \right\} d^3\vec{r} \\
&+ \frac{\partial}{\partial D} \int_{V_3} \left\{ \hat{\varphi}_{\rm out}(\vec{r}) \left[\frac{(n+1)}{2} \frac{\rho_{\rm out} \beta}{M_{pl}} \right] - \frac{(2+n)\mu_{\rm out}^2 \hat{\varphi}_{\rm out}^2(\vec{r})}{4} \right\} d^3\vec{r} \\
&- \frac{\partial}{\partial D} \int_{V_2} \left\{ \hat{\varphi}_{\rm out}(\vec{r}\,') \left[\frac{(n+1)}{2} \frac{\rho_{\rm out} \beta}{M_{pl}} \right] - \frac{(2+n)\mu_{\rm out}^2 \hat{\varphi}_{\rm out}^2(\vec{r}\,')}{4} \right\} d^3\vec{r}\,';
\end{aligned}
\tag{40}
$$

where we used $T^m \approx -\rho$, and ρ_1 and ρ_2 are the densities of the *large* and the *test* bodies, respectively, and $\rho_{\rm out}$ is the density of the *environment* (i.e. the density outside both bodies). We stress that the terms quadratic in the field appearing in Eq. (40) are *not* negligible in comparison to the corresponding linear terms, as our detailed numerical calculations show. In fact both terms turn out to be of the same order of magnitude.

In the last two integrals of Eq. (40), we have to rewrite the chameleon in terms of the corresponding coordinates adapted to each body [32–35]. Moreover, we neglect the contribution of the second part of $\hat{\varphi}_{\rm out}$ given by $\sum_{lm} C_{lm}^{\rm out2} k_l(\mu_{\rm out}r')Y_{lm}(\theta',\varphi')$, to the last integral [i.e. we take $\hat{\varphi}_{\rm out}(\vec{r}\,') \approx \sum_{lm} C_{lm}^{\rm out1} \sum_{w=0}^{N} \alpha_{w0}^{*l0} i_w(\mu_{\rm out}r')Y_{w0}(\theta',\varphi')$] because that contribution turns out to be negligible in comparison with the other one.

Each integral of the above equation has a linear term in φ and a squared term (φ^2). Therefore, we separate $F_{z\varphi}$ in two terms, a linear one $F_{1z\varphi}$ and a squared one $F_{2z\varphi}$ such that $F_{z\varphi} = F_{1z\varphi} + F_{2z\varphi}$. The final expressions for such terms that provide the chameleon mediated effective force on the *test* body are not very enlightening, and the steps leading to them are rather cumbersome and technical (see Appendix C). However, the most important point to be stressed, and which constitute the basic result of this paper, is that the expressions for $F_{1z\varphi}$ and $F_{2z\varphi}$ show an explicit dependence with the composition and size of the *test* body. Therefore, and as already noted, the WEP is violated in principle in these kind of models even in the case of an universal coupling.

In the next section we use these results in order to evaluate numerically the extent to which this effective force is suppressed by the *thin shell* effects in the two bodies, and also by other effects induced by the presence of additional objects in the setup. Then we estimate the Eötvös parameter and confront the outcome with the bounds imposed by the current data associated with the Earth based experiments and the LLR.

The general formulae that we have provided can be used for the evaluation of the force to any desired degree of precision. This can be done by following the steps we have presented in previous sections and by adjusting the level of approximations we have used. The approximations involved are of course the cut-off in the series expansion, which can straightforwardly be continued to any desired order.

V. APPLICATIONS

It is important to point out that the geometry of the actual Earth based experiments that have been used to test the WEP, such as those using torsion balances is much more complex than what our simple model depicts. In particular, the inclusion of the other material bodies that are present in the laboratory near the torsion balance could drastically modify the effective chameleon force acting on the *test* bodies, and their incorporation might led to important changes in the theoretical predictions of the Eötvös parameter. For instance, the environment that separates the torsion balance (that contains the *test* bodies) from the hill (which in the simple one body approach is the only source of the chameleon field) does not consist of just a vacuum and the Earth's atmosphere, but includes also a metal case and other objects located in the proximity of the experimental equipment. Those complications can often be ignored when one is considering linear fields which couple in a non-universal way to matter, and whose presence can led to effective violations of the WEP just as in the original Fifth Force proposals [36]. However, when dealing with highly non-linear models as the one studied here, the situation might be more complicated. Therefore one might need, in principle, a very detailed model for the actual ρ in the laboratory in order to take into account the true effect of the environment around the two bodies (the *large* body and the *test* body) used in the test of the WEP. This would require the modeling of the matter distribution in great detail, and then facing the very difficult task of solving a

complicated non-linear partial differential equation with a rather intricate boundary conditions. In order to advance in this direction and to make the calculations feasible, we are forced to ignore some of these complications while incorporating in the modeling of the situation some of the most important features of the experiment. For instance, we have analyzed the extent to which different environments affect the resulting chameleon force between the two bodies.

In the following we will proceed in two stages. In the first one we consider the simplest model for ρ as given by Eq. (8). First we take two type of environments represented by ρ_{out}: one is given by the chamber's vacuum density, and the other is given by the Earth's atmosphere. In the second stage we reanalyzed the results of the first stage, after taking into account, in a self-consistent manner, the encasing's material (which we consider to be of spherical shape) around the *test* body, as a manner to more accurately characterize the vacuum chamber used in the Eöt-Wash experiment that shields the test bodies (see Sec. V A 2) [18]. Regarding this point, we need to emphasize that, in previous works [25], the contribution of this metal encasing has been modelled together with the two bodies, the low density environments and the metal encasing as planar slabs (in contrast to our more realistic modeling based on spherical like objects). That is, the setting used in [25] corresponds to a "one dimensional planar" model[19].

Now, in the scenario where one does not consider such metal casing, the model could be applied to at least two kind of experiments: i) a laboratory experiment similar to the Eöt-Wash experiment but without the metal shell. This scenario, as far as we know, has not been implemented in an actual high precision Earth based experiment, and therefore our estimates cannot be used directly, at this time, to set relevant bounds. However, combined with rough estimates of the suppression effects, these already show that the appearance of the *thin shell* effects are by themselves insufficient to suppress the observable violations of the WEP for some values of the parameters; ii) an actual space-based experiment like the LLR where the Sun plays the role of the *large* body and the Earth or Moon represent the *test* bodies. For this second situation the use of our analysis would mean one is neglecting the effects of an actual *three body problem* where the Sun, the Moon and the Earth collectively determine the scalar-field. A much more precise study would require taking the effects of these three bodies into account simultaneously and self-consistently. We have not done so and instead have relied on an analysis based on two body system as an approximation. We consider this to be a reasonable approximation due to the fact that despite the intrinsic non-linearity of the model, the change due to the presence of the Earth on the value of the scalar field at the Moon's surface is sub-leading to that of the Sun. Thus, in our estimates, when computing the acceleration of the Earth towards the Sun we neglect the presence of the Moon and viceversa. This by the way, is a standard approximation used widely in the community studying these questions.

Now we illustrate the usefulness of the analytic expressions for the force in situations of experimental relevance.

A. The Eöt-Wash Torsion Balance Experiments

1. An idealized experiment without a vacuum chamber

One the most precise experiments on this line consists of a continuously rotating torsion balance which is used to measure the acceleration difference toward a large source (like the Earth, a lake, or a mountain) of *test* bodies with the same mass but different composition. In addition, as we have already mentioned, the Eöt-Wash experiment includes a vacuum chamber that encases the test bodies, and which is shielded by a metal encasing. We shall first consider a model of a simplified "Eöt-Wash" scenario where the metal encasing is absent (or ignored). The set up considered in previous sections correspond to this idealized experiment. Despite the fact that such scenario does not represent the realistic experimental set up at present, we have decided to consider it in order to motivate the realization of an experiment that avoids the inclusion of such vacuum chamber encasing, providing the theoretical bounds one might be able to achieve by a relatively simple modification of the current experiment.

Thus we will compute the Eötvös parameter associated with the differential acceleration of two bodies of different composition. This parameter is given by $\eta \sim 2\frac{|\vec{a_1}-\vec{a_2}|}{|\vec{a_1}+\vec{a_2}|}$, where $\vec{a_i} = \vec{a}_{i\varphi} + \vec{g}$ ($i = 1, 2$) is the acceleration of the $i-test$ body due to the chameleon force $\vec{a}_{i\varphi}$, and the force of gravity $\vec{g}$, which is basically due to the gravitational field produced by the *large* body. The acceleration $\vec{a}_{i\varphi}$ on the small body is computed using Eq. (40).

As we emphasized before, in all the cases that we have analyzed we find that, the linear and the quadratic terms of the chameleon field in the expression of the total energy (and hence the force) are comparable, so neither of them can

---

[18] We thank P. Brax for calling our attention to this aspect of the experiment.
[19] It should be noted that the analysis of Ref. [25] is devoted to the torsion pendulum experiment rather than the torsion balance here considered. Needless is to say that the two are not exactly the same.

be ignored. In most cases, the "optimal " cutoff N in the series expansion, estimated as the integer part of N_0 turns out to be zero (cf. Section II B). Thus, we keep only the first term of each sum so as to avoid numerical instabilities. The value for N required to improve the accuracy in the solution increases with increasing n and β, the effect being more pronounced for dependence on n. Furthermore, the value of N also increases with the density of the outside medium ρ_{out}. In fact, in some cases, the value needed for N is so large that it effectively impedes the calculation.

Moreover, regarding the summations over the infinite ranges for l and w in the series of Eq. (C5) we have checked the rate of convergence and found that one obtains basically the same result when cutting off the sums at $w = 4$ and $l = 4$ than when taking only the dominant terms $l = 0$ and $w = 0$ (the relative difference between both calculations in the predicted value of the Eötvös parameter, namely on the value of $\frac{\Delta\eta}{\eta}$ is of order 5×10^{-3}) . The reason for this is that when l increases, k_l also increases but i_l decreases very rapidly. The main point is that the quantity C_l decreases faster with l than the corresponding rate of growth of k_l. In Appendix A we show, that the results obtained for $N = 4$ and taking the summations up to $l = 4$, are the same as those presented in this section. We have been able to perform calculations up to N = 20 and we have observed that the first terms, those corresponding to $l = w = 0$ are the ones representing the main contributions to the results.

On the other hand, in the Appendix B we study the *test-particle* limit by taking $R_2 \to 0$ as ρ_2 is kept constant, and analyze how the violations of the WEP in the Eötvös parameter are suppressed by the presence of a thin shell. In particular, this occurs even when the coupling is *not* universal.

One of the most stringent bounds regarding the possible violations of the WEP is found when comparing the differential acceleration of two *test* bodies (e.g. two test-balls of Beryllium and Aluminium) using the Earth or its local inhomogeneities, as the source of the acceleration; the experimental value is $\Delta a_{Be-Al} = (-2.5 \pm 2.5) \times 10^{-15} \text{m/s}^2$ [10]. As discussed in Refs. [10] and [37], there are two sources for the relevant signals in short-range effects: a hillside of 28 m located close to the laboratory, and a layer of cement blocks added to the wall of the laboratory of 1.5 m (we estimate 1 m distance between the wall and the device). We model the short range sources by spherical masses at a given distance and consider only the contribution of the hillside, such as in Ref. [38]. For such a configuration, the differential acceleration on two *test* bodies due to the hill produces an Eötvös parameter $\eta_{Be-Al}^{hill} = (-3.61 \pm 3.47) \times 10^{-11}$. In order to characterize such a configuration in our expression for the force, we make the following assumption for the *test* bodies: for the masses we take $m_{Be} = m_{Al} \approx 10$ g and for the densities $\rho_{Be} \simeq 1.85 \text{g cm}^{-3}$, $\rho_{Al} \simeq 2.70 \text{g cm}^{-3}$, and $\rho_{hill} \simeq 9.27 \text{g cm}^{-3}$. We consider the bodies as surrounded by an environment of constant density ρ_{out} and take two values for this density (so that people may compare actual and possible experiments): i) the density of the vacuum-chamber $\rho_{out} = 10^{-7} \text{g cm}^{-3}$; ii) the density of the Earth's atmosphere $\rho_{out} = 10^{-3} \text{g cm}^{-3}$.

In addition, for the mass M that appears in the chameleon potential [cf. Eq. (3)] we take also the value $M = 2.4$ meV which, as mentioned before, corresponds to the cosmological chameleon.

In Figure 7 we show the predictions for the Eötvös parameter η calculated with the method developed in this paper together with the predictions of the standard approach . For this latter, and following [1, 21, 43] (among others), we use the following expression for the total force (gravitational plus chameleon field) between two bodies A and B,

$$F_{AB} = (1 + 2Q_A Q_B) F_N, \tag{41a}$$

$$Q_C = min\left(\beta, \frac{|\varphi_\infty - \varphi_{C min}^{in}|}{2M_{pl}\Phi_N}\right), \tag{41b}$$

where F_N refers to the gravitational force between A and B, $\Phi_N = \frac{G\mathcal{M}_C}{R_C}$ refers to the Newtonian potential of the body C. We considered the two different values for the density of the environment mentioned above[20]. The difference between our prediction and those calculated by other authors are due to two main reasons: i) other authors do not compute the field configuration for the two body problem as done in this paper, instead they estimate the chameleon mediated force of the *large* body on the *test* body by considering the effects of the field only due to the *large* body, and then they compute this force by using the gradient of the field at the location of the point-like test body and

---

Table I: Thin shell condition for different test bodies surrounded $\rho_{\text{out}} = \rho_{\text{vacuum}}$ and $M = 2.4$ meV

n	β_{Be}	β_{Al}
(1)	(2)	(3)
1	3.16	1.78
2	0.46	0.32
3	0.13	0.10
4	0.056	0.032

Values of the couplings β (columns (2) and (3)) associated with a given n (column (1)) below which the *thin shell* condition is no longer satisfied within Al and Be test bodies.

Table II: Thin shell condition for different test bodies surrounded by $\rho_{\text{out}} = \rho_{\text{atmosphere}}$ and $M = 2.4$ meV

n	β_{Be}	β_{Al}
(1)	(2)	(3)
1	0.15	0.10
2	0.043	0.032
3	0.040	0.030
4	0.010	0.0070

Values of the couplings β (columns (2) and (3)) associated with a given n (column (1)) below which the *thin shell* condition is no longer satisfied within Al and Be test bodies.

the characterization of that effect of the field on the small object through an estimation of an effective coupling [21] ii) other authors split the prediction into two cases: screened or unscreened *test* body considering only the effect of the *test body* when computing the force in an approximate way as described above. In the present work we amply the energy functional criteria described in Sec III in order to establish which of the approximate configurations provides a more accurate characterization of the situation in each case. In particular our own treatments are based on the quadratic approximation to the effective potential in each region, but as indicated by the energy functional criteria, the results so obtained are not always the most accurate among the existing ones, and for some situations and values of the model's parameters the standard results are more trustworthy than ours. However, we have also found that in various situations our analysis yields approximations to the chameleon field profile that are better that those obtained in the standard approaches. In those cases our results are more trustworthy than the previously existing ones. Tables I and II show, for various values of the exterior medium's density, the values of n and β for which the *test* body (made of Al and Be) transitions from satisfying the *thin shell* condition to failing to do so. Furthermore, we use the energy criterion developed in Sec.III to determine when the solution obtained by the methods of this paper is better than the one obtained by the standard approach to the problem at hand. We note that these approximations can be improved by turning to something like a *thick shell* approximation for the *test* body potential, while still working with the scalar field's equation for the full two body problem [22]. We will present the results obtained by such refined calculations in a forthcoming paper [26]. In this paper, our treatment includes cases in which the *test* body has and

---

[21] For instance, Khoury & Weltmann [1] use the *test particle* limit to estimate the force, Brax et al .[22] use the superposition principle to calculate the force, Puetzfeld & Obukov [30] consider the *test particle* limit, Mota & Shaw [19] consider two infinite parallel planes, Tamaki & Tsujikawa [28] consider the *test* bodies as *test particles* with the acceleration of the *test particle* proportional to an effective coupling of the field to the *test* body; and therefore miss the contribution of the *test* body on the chameleon field.

[22] For the situations we have studied in this work, the *large* body is always screened for $M = 2.4$ meV and the considered values of n and β.

Table III: Thin shell condition for the mountain surrounded by $\rho_{\text{out}} = \rho_{\text{atmosphere}}$ and two test bodies surrounded by $\rho_{\text{out}} = \rho_{\text{vacuum}}$ and $M = 10$ eV

n	β_{mountain}	β_{Be}	β_{Al}
(1)	(2)	(3)	(4)
1	10	10^7	10^7
2	1	10^6	10^6
3	0.01	10^5	10^5
4	0.01	10^4	10^4

Values of the couplings β associated with a given n (column (1)) below which the *thin shell* condition is no longer satisfied within the mountain (column (2)), and within the Al and Be test bodies (columns (3) and (4))

does not have *thin shell*. For instance, for $n = 1$, the *thin shell* condition is satisfied for $\beta > 0.1$. On the other hand, it is well known that the change between the screened and the unscreened case is smooth and it is not well described by the standard approach [21, 24]. The behaviour of the values of η estimated by other authors can be divided in two categories depending on whether the test body is screened (larger β) or not (lower β): η decreases sharply for lower β (unscreened *test* body) and slowly with increasing β (screened *test* body).

Let us summarize our results. In all the cases analyzed by us, η decreases as n increases. Furthermore, it is interesting to compare the effect of the density of the environment on the estimated values of η: for a fixed value of n and β when the density of the environment *increases* by several orders of magnitude, the value of η *decreases* by several orders of magnitude. On the other hand, the values of η are drastically different from the ones obtained using the standard approach for $\beta < 10^{-2}$ and $1 \leq n \leq 4$, while there are differences in two or more orders of magnitude for $\beta > 10^{-2}$.

2. The model including the metal encasing

It has been pointed out [25, 39–41], that the effect of the metal encasing of the vacuum chamber is determinant for the outcome of experiments that includes such kind of devices. Therefore, we have made explicit calculations for η by taking into account the metal shell surrounding the *test* body (see Fig. 8). In order to compare with other predictions found in the literature we consider first the scenario where the density outside the *larger* body is equal to the density inside the vacuum chamber (see Fig. 9) and then analyze the more realistic situation where the density inside the vacuum chamber is $\rho_{vac} = 10^{-7}$g cm^{-3} and the density outside the *large* body is equal to the Earth's atmosphere at sea level $\rho_{out} = 10^{-3}$g cm^{-3} (see Fig.10). The effect of the metal encasing in the standard approach has been estimated by multiplying the value of η (obtained without the encasing) by the suppressing factor found by Upadhye [25]. That is, $\eta_Y = \text{sech}(2m_{\text{shell}}d)\eta$, where η_Y corresponds to the value of η when taking into account a Yukawa-like suppression that accounts roughly for the effect of the vacuum chamber walls which have the following parameters: $m^2_{\text{shell}} = \frac{n(n+1)M^{n+4}}{\varphi_{\text{shell}}^{n+2}}$ and $\varphi_{\text{shell}} = \frac{nM^{4+n}M_{pl}}{\beta\rho_{\text{shell}}^{1/(n+1)}}$. In particular we used the values $d = 1$ cm and $\rho_{\text{shell}} = 10$ g cm^{-3}, for the thickness and density of the metal encasing, respectively. Let us remind that in the work of Upadhye [25], the *larger* body, the *test* body, the metal encasing around the *test* body, and the environments are all modeled by *planar slabs*[23]. The Yukawa-like suppression factor used by other authors was found by fitting the numerical results to an analytical function. It should be noted that this is just an approximation to the calculation and that a more accurate estimation would be obtained by considering the joint effects of the *larger* body, the *test* body and the metal shell. We improved this approximation by including the shell in our previous setup in a self-consistent fashion. In Appendix D we check the results of our method when considering the complete experimental setting (with the full description of metal encasing). We compare these latter results with our estimates of η without considering the metal shell but introducing a multiplicative factor corresponding to a Yukawa suppression in the expression of the acceleration. It follows that the difference is very small (see Fig. 15).

---

[23] We remind the reader again the analysis of Ref.[25] was performed to model the torsion pendulum rather than the torsion balance.

As noted before, we were unable to apply the energy criterion proposed in Section III to determine if our solutions are better than the ones proposed by the standard approaches because in those, the scalar field configurations of the present experimental setup have not been calculated explicitly. Even though there are numerical results of the one body problem surrounded by a metal shell, these can not be directly applied to the experimental setup considered here, since for the present experimental device the large body is outside the vacuum chamber and the test body is surrounded by a metal encasing. Among other problematic issues, the experimental device analyzed here does not have the spherical or planar symmetries of the situations that have been explicitly analyzed in the literature [25, 40, 41]. On the other hand, we have shown in Section III that for $M = 2.4$ meV the energy criterion for the full fledged problem indicates that the solution for the field configuration obtained without explicitly modeling the encasing that was obtained in this paper must be preferred over the one obtained by standard approach, while for the case $M = 10$ eV the same happens only for a rather restricted range of values of β. Table III shows, for each fixed value of n, the values of β for which the energy criterion favors the solution obtained by our method. Hence we used the energy criterion for the two body problem without encasing to restrict the range of the values of model's parameters for which our method yields trustable estimates of the values η to be used in comparisons with the observational bounds. Fig. 10 left shows, for each trustable value of n and β, the results for the corresponding values of η. For the rest of the cases, we expect to obtain the appropriate estimates, by considering some type of *thick shell* approximation to the effective potential, in future works [26].

We found that for some values of n and β, our estimates for the values for η are above the experimental bounds in contrast with the results by other authors. The main reason for this discrepancy is because other approaches estimated η without considering the suppression due to the metal encasing *ab initio*, which is already several order of magnitude below our predictions (see Fig. 7). In other words, the results by other authors are based on the suppression of an initially underestimated "bare" value of η.

On the other hand, it follows from the comparison of Figs. 7 and 10 that for $M = 2.4$ meV and $\beta > 10^{-3}$ the intensity of the suppression is so important that it predicts no violation of the experimental bounds for η, while for $M = 10$ eV the suppression effect becomes relevant only for $\beta > 10$. Nevertheless, the method developed in this paper allows us to establish the following constraints : i) for $M = 2.4$ meV and $n = 1$ the range $10^{-5} < \beta < 10^{-2}$ is excluded; for the same M and $n = 2$ the range $10^{-5} < \beta < 10^{-3}$ is excluded too ;ii) for $M = 10$ eV and $n = 1$ the range $10 < \beta < 10^4$ is excluded; for the same M and $n = 2$ the ranges $1 < \beta < 10^3$ are excluded; for the same M again and $n = 3$ the range $10^{-2} < \beta < 10^3$ is excluded and finally for $n = 4$ the range $10^{-2} < \beta < 10^2$ is excluded as well. Some of these values were already excluded by other authors[25, 42], but other values were not. Furthermore, Fig. 10 shows that as M increases, the experimental bounds on η can rule out larger values for n and β. Finally, it is worth stressing that the above estimations are based on modeling the vacuum chamber as a *spherical* metal encasing and the detailed consideration of any asymmetry of the experimental device might change the results in a important manner, in one direction or the other. That is, the details of the geometrical arrangement might led to an increase or a decrease in the expected value of η.
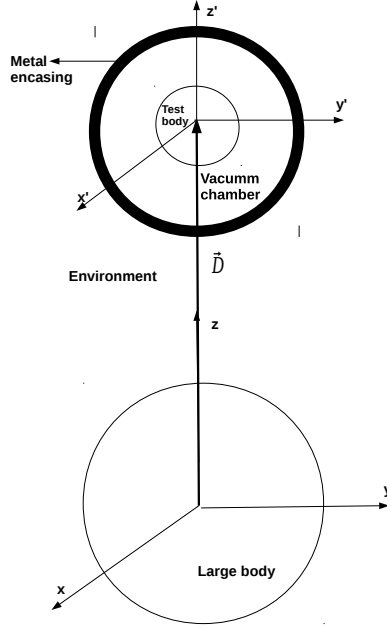
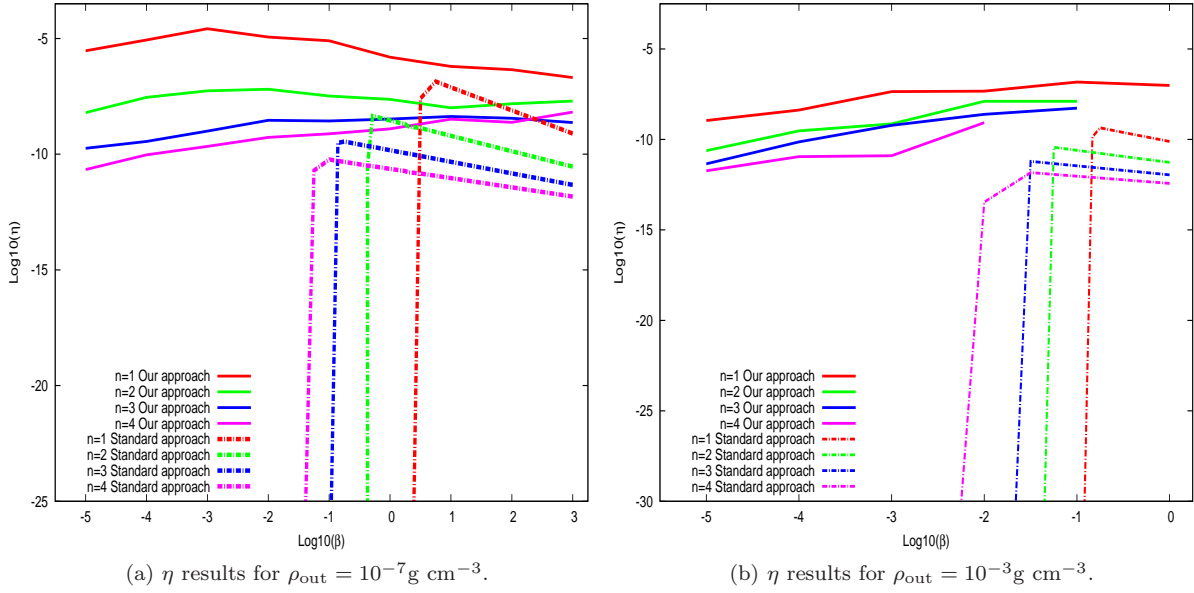Figure 8: The two body problem including the metal encasing of the vacuum chamber.

(a) η results for $\rho_{\text{out}} = 10^{-7}\text{g cm}^{-3}$.

(b) η results for $\rho_{\text{out}} = 10^{-3}\text{g cm}^{-3}$.

Figure 7: The Eötvös parameter η (in $\log_{10}$ scale) as a function of the parameter β (in $\log_{10}$ scale) for different positive values of n and $M = 2.4 \times 10^{-3}\text{eV}$. The density of the environment ρ_{out} is assumed to be equal to: Panel (a) the vacuum's density inside the vacuum chamber $\rho_{\text{out}} = 10^{-7}\text{g cm}^{-3}$; Panel (b) the Earth's atmosphere density $\rho_{\text{out}} = 10^{-3}\text{g cm}^{-3}$. The predictions computed by Khoury & Weltman [1] are also included and labeled as the *standard approach*
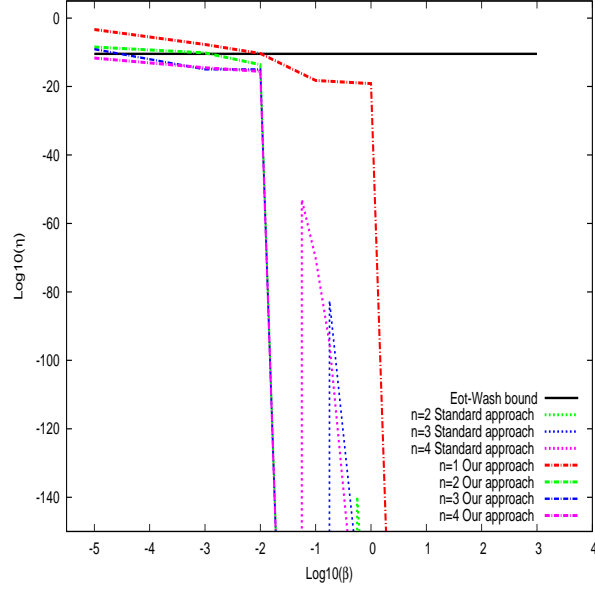
Figure 9: The Eötvös parameter η (in $\log_{10}$ scale) as a function of the parameter β (in $\log_{10}$ scale) including the metal encasing of the vacuum chamber as depicted in Fig. 8 for different positive values of n. Here we assume that both the density of the environment surrounding the Earth and inside the vacuum chamber are $\rho_{\text{out}} = 10^{-7}\text{g cm}^{-3}$. Also shown are the predictions computed by Khoury & Weltman [1] with the effect of the metal encasing modeled by multiplying their estimates of η by the factor $\text{sech}(2m_{\text{shell}}d)$.
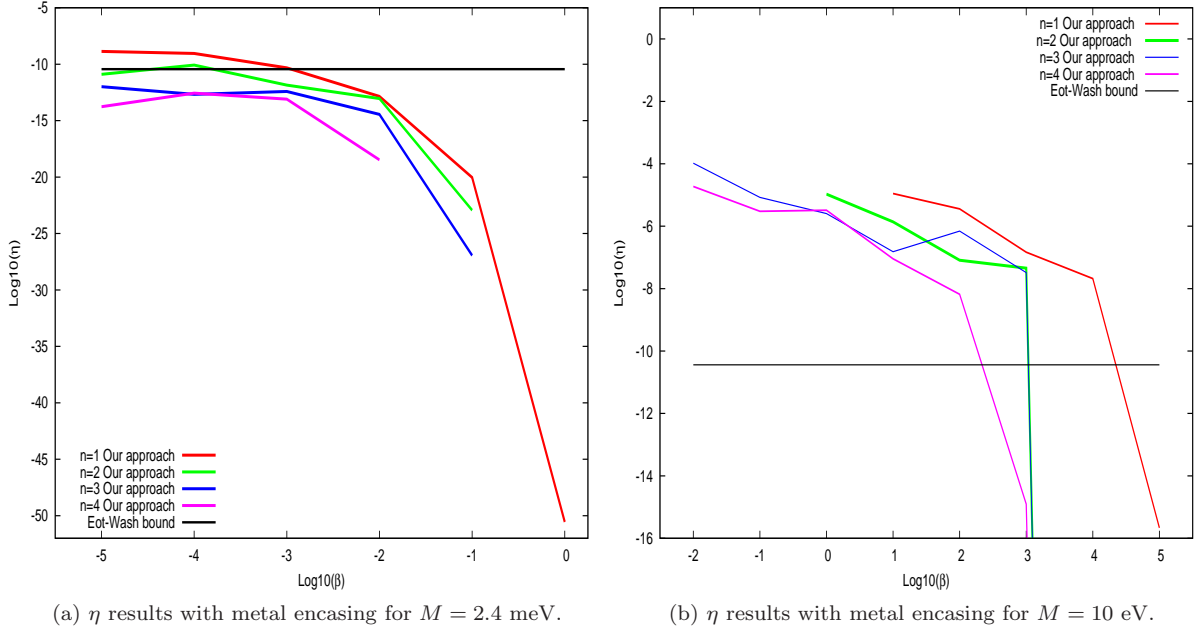
(a) η results with metal encasing for $M = 2.4$ meV.

(b) η results with metal encasing for $M = 10$ eV.

Figure 10: The Eötvös parameter η (in $\log_{10}$ scale) as a function of the parameter β (in $\log_{10}$ scale) including the metal encasing of the vacuum chamber as shown in Fig. 8 for different positive values of n. The density of the environment surrounding the Earth ρ_{out} is assumed to be equal the Earth's atmosphere density $\rho_{\text{out}} = 10^{-3}\text{g cm}^{-3}$; the density of the environment inside the vacuum chamber is assumed to be $\rho_{\text{vac}} = 10^{-7}\text{g cm}^{-3}$; Left: $M = 2.4$ meV (cosmological chameleon); Right: $M = 10$ eV.

B. Lunar Laser Ranging Experiments

Another setting that serves to test the WEP is the LLR which, since 1969, has provided high-precision measurements of the Earth-Moon distance [44]. Reflectors placed on the lunar surface allow the measurement of the round-trip travel time of short pulses of laser light, and thus set limits on the differential acceleration of the Earth-Moon system in free fall towards the Sun.

In previous studies [1, 28, 45], the chameleon effect has been analyzed using the free-fall acceleration of the Moon and the Earth towards the Sun by assuming a constant solar density. We will base our analysis on the same approximation for simplicity in order to apply the methods developed in the preceding sections and also because as we will next argue the approximation should be a very good one. Although the solar density is far from being constant within the Sun's interior (varying over several orders of magnitude from the center to the Sun's surface), one does not expect that the results of the analysis are altered significatively for the situation at hand. The fact is that, as shown in those works, even when one describes the Sun in terms of a collection of infinitesimal volumes, one finds that contributions from the Sun's deep interior become exponentially suppressed due to the large mass of the chameleon (given that as the density increases, so does the effective mass of the chameleon, and thus the effective range of the field decreases) leading to a situation where the field in the Sun's exterior is in fact determined to a very large extent by a *thin shell* of matter near the Sun's surface. As the chameleon field in regions very close to the Sun's surface do not suffer from such a large suppression, one finds that when focusing on the external field, the approximation where the field is taken to be as generated almost entirely by this *thin shell* (while the effect of the rest of the Sun is sub-dominant [1]) becomes a very good one. In fact the actual numerical calculations show that for the vast majority of values for n and β (including the ones that we will be interested on), the solar chameleon field at very far locations is well estimated by that approximation. On the other hand, when considering the force on the small object while looking for violations of the UFF, the details of the scalar-field profile in the object's interior are important, and in particular, the charged-conductors analogy indicates that it is essential to take into account the anisotropy of the chameleon field within the small body's interior, that results from the presence of the *large* body outside. This should be clear when noting that it is just only due to that anisotropy that a force on the small body, directed towards the *large* body, results from the scalar field interaction with the small body. Finally, we stress that given the very small ratio between the Sun's size and the Sun-Earth or Sun-Moon distances, the non-linearities that are important in the Sun's interior can be expected to play no significant role in determining, together with the small body (Earth/ Moon), the behaviour of the scalar field in the neighbourhood of such small body. In view of all the above arguments, it seems reasonable to take the Sun's density as its average density (as is usually done in such analysis ([1, 28, 45]). In a near future we hope to drop this assumption and study the chameleon two body problem, in even more detail, by developing appropriate analytical and numerical methods. Only such detailed study can determine in a completely unambiguous manner the extent to which the assumption about the homogeneity of the Sun's density is in fact a good approximation or a bad one.

Figures 11 and 12 show the predictions for η based on the LLR experiment. For this scenario we are considering the Sun as the *large* body ($\rho_{SUN} = 1.43$ g cm^{-3}, $R_{SUN} = 7 \times 10^8$ m) and the Earth or the Moon as *test* bodies with the following properties, respectively, $\rho_E = 5.5$ g cm^{-3}, $R_E = 6.371 \times 10^6$ m, $\rho_M = 3.34$ g cm^{-3}, $R_M = 1.737 \times 10^6$ m. Furthermore, we assume that all bodies are surrounded by an environment of constant density equal to the density of the interstellar medium. It is interesting to note that for $M = 2.4$ meV (see Figure 11) the difference between the resulting predictions from our model and those obtained by other authors is at most one or two orders of magnitude, while for the torsion balance experiments, the differences were more important, particularly for the cases in which the *test* body is unscreened. On the other hand, when considering $M = 2.4$ meV, the predictions indicate no conflict with the existing LLR tests for violation of the WEP for any of the values of n and β considered here. Again, as in the torsion balance experiment, there is an enhancement of η for increasing value of M. In fact, Fig. 12 shows that for $M = 10$ eV, the bounds resulting from LLR can be used to discard the values of β in the range $10^{-2} < \beta < 10^5$ when $n = 1$ and $10^{-7} < \beta < 1$ when $n = 2$. Some of these values were already excluded by other authors[25, 42], while others are ruled out, for the first time, with the present analysis. We remind the reader, that we have used the energy criterion discussed in Section III in order to establish when we can trust the results obtained by the method of this paper (which relies on the *quadratic* approximation to the effective potential) over those of the traditional approach for the estimates of η in various specific situations. For the case $M = 2.4$ meV we have found that the energy functional is always smaller for the field configuration obtained with our approach than for the one obtained in the standard approach. For the case $M = 10$ eV the energy criterion favors our results only for the values of β where the *thin shell* condition holds for the Sun. Accordingly, the results shown in Fig. 12 are restricted to the corresponding values of n and β.

On the other hand, the discrepancy in the value of η between our approach and the standard one is negligibly small for $M = 2.4$ meV, while there are important differences for the case $M = 10$ eV depending on the value of n and β.
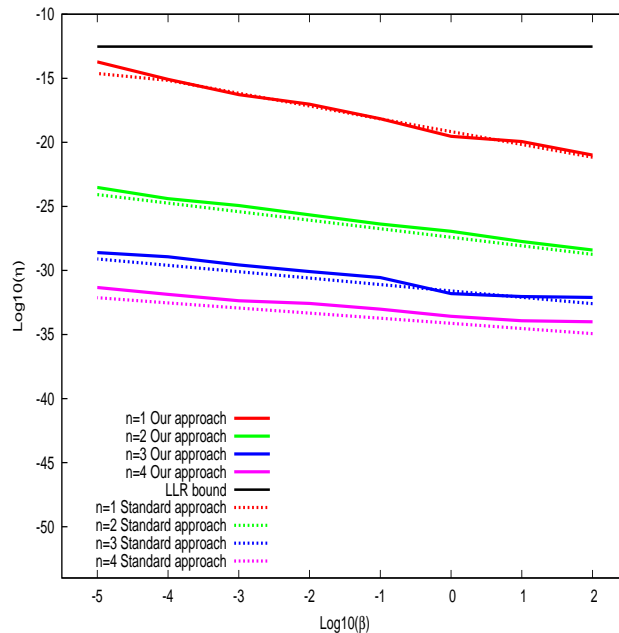
Figure 11: The Eötvös parameter η (in $\log_{10}$ scale) for the LLR experiment as a function of the parameter β (in $\log_{10}$ scale) for different positive values of n. All bodies are surrounded by the interstellar medium. $M = 2.4$ meV (cosmological chameleon). In all cases we compare the results of the calculations performed in this paper with the predictions computed by Khoury & Weltman [1].

Fig. 13 shows the region in the plane $n - \beta$ where the differences are significant.

In summary, in the last two subsections we have analyzed the predictions of the effective violation of the WEP that would result from the chameleon mediated forces in the model by considering different possibilities for the outside medium and different values for M, by using Eqs. (C3) and (C5), and compared our results with the experimental bounds obtained from the Eöt-Wash experiment. We realized that when adding the effect of the metal encasing, a Yukawa-like suppression leads to a significant change in the estimates. For some values of the parameters ($\beta > 10^{-3}$) the corrected predictions are within the bounds imposed by the actual Eöt-Wash experiment. These results suggest that it would be very interesting to carry out experiments of this type with no suppression due to encasing, as they would probably lead to significant improvement of the bounds on the chameleon model's parameters. In addition, we considered the LLR experiment, where there is no such suppression and found that in this setting there would have been an observed violation of the experimental bounds in the range $10^{-2} < \beta < 10^5$ when $n = 1$, and $10^{-7} < \beta < 1$ when $n = 2$, for a fixed $M = 10$ eV.

C. Comparing bounds from other experiments

Recently, Burrage & Sakstein [42] reanalyzed the constraints imposed on the chameleon models using different astrophysical and laboratory data, and found the bounds on the parameter space associated with the plane $n - \beta$ (fixing $M = 2.4$ meV) and $M - \beta$ (fixing $n = 1$). Using our analysis we also obtained complementary bounds on those planes but by considering data related with the Eötvös type of experiments using a torsion balance and the LLR experiments. We find that the region excluded by our calculations in the $M - \beta$ plane was in fact already excluded by other experiments [20, 25, 39, 46–49]. On the other hand, we can exclude a new region in the $n - \beta$ plane by fixing M to the cosmological value of the chameleon. Fig. 14 shows the bounds in the $n - \beta$ plane obtained in this paper using the torsion balance experiment (new constraints using LLR were also obtained but only for $n = 2$) together with the combined constraints presented in Ref. [42] [24]. We would like to stress that in the present analysis we have relied

---

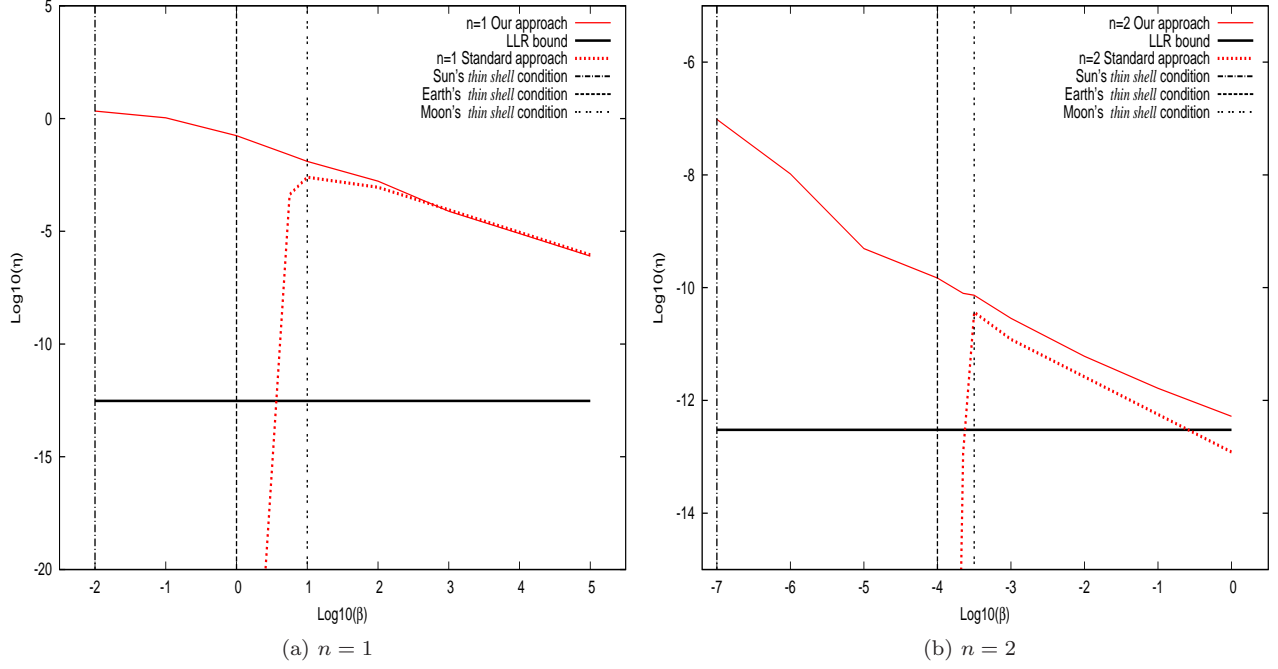[24] We thank J.Sakstein and C. Burrage for providing a modified plot to include our bounds.

(a) $n = 1$ (b) $n = 2$

Figure 12: The Eötvös parameter η (in $\log_{10}$ scale) for the LLR experiment as a function of the parameter β (in $\log_{10}$ scale) for different positive values of n. All bodies are surrounded by the interstellar medium. $M = 10$ eV. The vertical lines show the values of β below which the *thin shell condition* is no longer satisfied for the Earth, Moon and Sun. For all values computed in this plot, the energy criterion developed in Section III indicates that our approximation to the effective potential is better than the one used by the standard approach

.
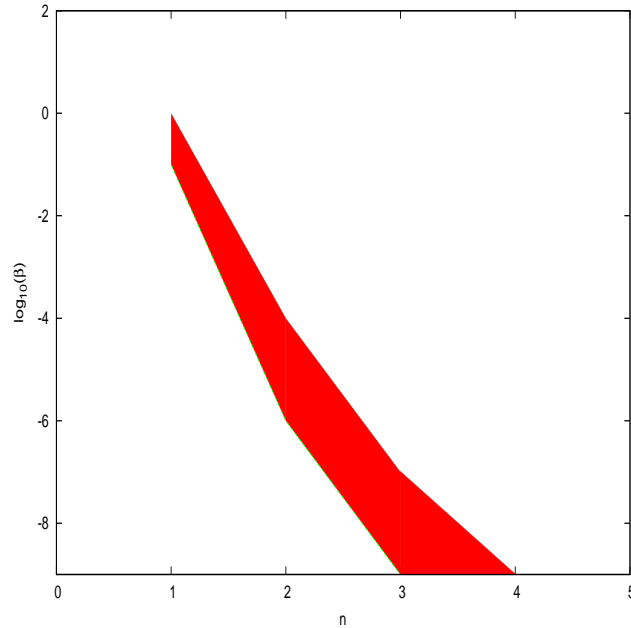
Figure 13: The shaded region in the figure shows the values in the $n - \beta$ plane where our approach has significant differences with the standard approach in the value of η for the LLR experiment with $M = 10$ eV.
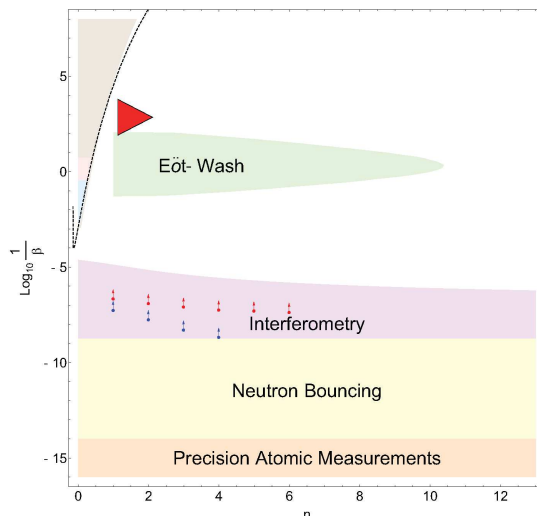
Figure 14: Bounds in the $n - \beta$ plane obtained in this paper (in red) using the torsion balance experiment with combined constraints compiled by Sakstein & Burrage. Here $M = 2.4 \, \text{meV}$.

on the *quadratic* approximation to the effective potential, even for cases when the *thin shell* condition is not satisfied by the *test* body. The reason for this is that in many such cases the energy criterion indicates that our solution is a better approximation to the scalar field solution for the specific problem than the one proposed by the standard approach in the case where no encasing of the vacuum chamber is considered. The lack of explicit calculations for the field configuration resulting from the standard approach is the reason why we could not apply the energy criterion discussed in Section III to the present situation. In a forthcoming paper[26], we expect to explore the situation using some adaptive approximation approximation to the effective potential within the *test* body for the relevant values of the model's parameters. We expect relatively small variation for the resulting estimates of η which will not change the overall picture in a significant way. We recall at this point that the most stringent bounds in the $n - \beta$ plane are imposed by the following experiments: i) The torsion pendulum of the Eöt-Wash experiment which has been used to probe fifth forces on sub-millimeter scales [25], ii) Atomic interferometry [39], iii) Ultra cold neutron bouncing [50] and iv) Atomic Precision Tests [23].

VI.   SUMMARY AND CONCLUSIONS

In this paper we examined, in a critical manner, the degree to which the chameleon models evade existing bounds on the violation of UFF as a result of the famous *thin shell* effects. We were motivated by the fact that any *extended* body that can modify the chameleon field to such a large extent so as to generate that kind of nontrivial behaviour of the field near their surface, cannot be considered as a "bona-fide" test particle. We have addressed the issue with a new method that allows the precise calculation of the full fledged two body system and its interaction with the chameleon field. This has allowed us to evaluate the chameleon mediated force between these bodies and to determine the differential acceleration on two *test* bodies towards the larger one resulting from the chameleon mediated interaction. As a result, we compared our estimates with the outcome of the WEP experiments on Earth and put constraints on the parameter space of the model.

The approach that we have followed to compute the force takes into account the contribution of the two bodies (the larger and smaller ones) to the static field configuration everywhere in space. In order to simplify the calculations we have considered a scenario where the coupling between the chameleon field and the matter fields is universal.

We have restricted the conclusions extracted from present analysis to those cases where the effective potential can be well approximated by a quadratic expansion around its minimum. However, we have found that the condition that is taken to indicate that this approximation is reliable (namely the *thin shell* condition) is not always satisfied for the values of the model's parameters for the experimental situations considered here. Therefore, we have developed a criterion, based on an energy minimization test in order to determine in which cases the approximations we have obtained for the profile of the chameleon field in the two body problem is better than the approximation for the scalar field obtained by the standard approach. Consequently, we have decided to only trust the results of our method when the energy criterion indicates it is appropriate to do so. Results from Section III show that the method proposed in

Sect.II is not appropriate when the large body is *not* in the thin shell regime. However, when both bodies are in such regime or when just the test body fails to be in that regime, our approach continues to provide a better approximation than the one obtained with the standard approach. In a forthcoming paper[26], we expect to take one step forward and incorporate an adaptive approximation to the effective potential when appropriate, and thus to explore a wider range of values of the free parameters of the chameleon model. In such way we expect to set constrains for values of M, n and β that were excluded from the conclusions obtained in this work as a result of the indications coming from the energy criterion.

Furthermore, apart from the standard approximation made in characterizing the effective potential for the chameleon field as a quadratic one around its minimum, the relevant approximation that has been performed is to cutoff the series expansions of the development in spherical harmonics of the chameleon field. Other approximations were considered in order to model the hill, and the encasing of the vacuum chamber for Eöt-Wash experiment and the description of the outside media for each experiment (see Sect. V).

In the selection of the adequate cutoff in the series, we have followed the approach proposed in Refs. [34] and [35]. The approach then offers in principle a path for calculations to any desired order. We have found that the force on the *test* body *does* depend on the *test* body's size and composition, making the model susceptible to receive experimental constraints arising from tests of the WEP, and thus, our conclusions differ drastically from studies which claim that the chameleon force is strongly suppressed whenever the *thin shell* regime ensues. The specific origin of the difference between our calculations and the ones that predict no effective violation of WEP in chameleon models, is that in those works [1, 18, 19], it is assumed that the force mediated by the chameleon field would be automatically suppressed when the bodies involved are in the *thin shell* regime, to such an extent as to make the chameleon force experimentally irrelevant. By performing a careful and detailed calculation we have shown that this is not always the case.

Regarding the situation where the coupling between the chameleon and the matter fields is universal, we must remind the reader that, as discussed in the Introduction, it is only when test objects can be considered as true *point* particles which follow geodesics (as opposed to *test* extended bodies) that one might conclude that the model predicts absolutely no violation of the WEP. The point is, however, that such point *test* particles cannot be the ones that are associated with the *thin shell* effect, as such effect arises from a substantial influence of the body on the scalar field. The analysis of the level of validity of a direct extension of that notion to a realistic (and necessarily extended) body is highly non trivial. The calculations performed in this paper show that this issue is a rather delicate one and in particular that the conclusions that emerge from it can be particularly relevant for the case of chameleon models.

Furthermore, we have quantitatively estimated the differential acceleration for *test* bodies made of Be and Al for one of the most precise experiments yielding relevant bounds considering two possibilities for the outside medium, and found that the deviations from UFF might in principle be rather substantial. However, as it was pointed to us by a few colleagues and by a referee, the actual Eöt-Wash experiment makes use of a metal encasing that can substantially reduce the prediction for the observable effect. Consequently, we have carried out an additional analysis in which a model for such encasing is included leading to a solid estimate for the predicted values of the UFF violations and used those bounds to place further constraints on the model. It was important to compare the constraints emerging for our analysis with those obtained by other experiments that have set strong bounds on the parameters of the chameleon model. One of the most important results of this paper is that, using experimental bounds from the torsion balance experiment, we were able to put additional constraints on the parameters in the $n - \beta$ and $M - \beta$ planes beyond those placed by other experiments such as i) torsion pendulum, ii) atomic interferometry, iii) cold neutron bouncing and iv) precision atomic measurements. Thus, our analysis concludes that i) for $M = 2.4$ meV and $n = 1$ the new excluded values are $10^{-5} < \beta < 10^{-2}$, and when $n = 2$ the range $10^{-5} < \beta < 10^{-3}$ is excluded as well; ii) for $M = 10$ eV and $n = 2$ the new excluded values are $1 < \beta < 10^3$; when $n = 3$ the range $10^{-2} < \beta < 10^3$ is now excluded and finally for $n = 4$ the range $10^{-2} < \beta < 10^2$ is now ruled out.

Nonetheless, in contrast to previous works [1, 18, 19, 21, 25] which led to the conclusion that the *thin shell* effect in high density environments is precisely what prevents the chameleon model to be in conflict with the UFF, our work indicates that the absence of conflict between predictions of violations of the WEP and the Eötvös-like experiments arises essentially from the Yukawa-like suppression due to the vacuum's chamber metal shell. This observation should serve as strong motivation for our experimental colleagues to devise suitable laboratory arrangements. For instance, the construction of experimental setups without the metal encasing or other arrangements that avoid strong Yukawa like suppressions can open the path for obtaining constraints on this class of models that are more stringed than the existing ones. In summary, experiments where neither the *large* source nor the *test* bodies are placed within any kind of encasing seem, in principle, to be better alternatives to be used in tests of violations of the WEP than current versions of the Eöt-Wash type experiments. An example of such a set-up is the Microscope Satellite [53] which was recently lunched. The estimated precision of η is improved by two orders of magnitude with respect to Earth-based experiments.

We have also considered the LLR experiment as a scenario where the encasing around the *test* bodies is absent, and found a new exclusion zone for the chameleon coupling, namely, $10^{-7} < \beta < 1$, when assuming $M = 10$ eV and

$n = 2$.

This work should alert colleagues who are under the impression that the chameleon or *thin shell* effect completely and effectively protects the model from having to confront the strict experimental bounds associated with the tests of violations of the WEP. In light of our results, the various models that rely on the chameleon effect should only be considered as viable for those specific values of M, n and β that are not ruled out by experiments. In this regard, it is important to emphasize that, just as in this case, extreme care is needed to asses the viability of other modified theories of gravity proposed to account for the accelerated expansion of the universe, and which often rely on the chameleon or *thin shell* effects in order to avoid the stringent bounds imposed by the *classical tests of general relativity*. In fact many of such theories have not been yet studied in detail in connection with the Eötvös type of bounds considered here, often because one takes for granted that the *thin shell* effects will suppress possible effective violations of the WEP. Moreover, a good segment of the community working in the field seem to be under the impression that such violations are not even present given the fact that metric alternative gravity theories incorporate universal couplings just as general relativity. That is, such alternative theories couple to matter universally, as the chameleon models considered in the present work, where we assumed that β is the same for all the matter species. In view of our results, the viability of those theories needs to be examined in detail. Various types of popular $f(R)$ gravity theories are affected by the previous discussion. The point is that even if the *thin shell* effect allows some those theories to avoid conflict with standard solar-system tests (as concluded by several authors [51]), the same mechanism can result in predictions of violations of the WEP which far larger than the experimental existing bounds as we have shown in this work. Therefore, in view of the present work, it would be prudent to reconsider the empirical viability of all such theories in the context of the WEP tests that we have analyzed with a novel approach.

Appendix A: The expanded solution

The results presented in Section V have been calculated taking only the first ($N = 0$, $l = 0$) terms in the truncated series for the expression of the force. Here we show that taking two more terms (up to $N = 4$, $l = 4$), the results are basically the same. We only take two more terms because the larger the number of terms the more unstable the numerical calculation becomes. On the other hand, the terms in the summations decrease several orders of magnitude when $l \neq 0$ and $w \neq 0$, so they do not really contribute to the result. Eqs. (18), (22), (26) and (27) yield

$$b_1 \delta_{l0} = C_l^{\text{out1}} a_l + \sum_{w=0}^{4} C_w^{\text{out2}} z_{wl}, \tag{A1a}$$

$$b_2 \delta_{l0} = C_l^{\text{out2}} x_l + \sum_{w=0}^{4} C_w^{\text{out1}} y_{wl}, \tag{A1b}$$

$$C_l^{\text{in1}} i_l'(\mu_1 R_1) = C_l^{\text{out1}} k_l'(\mu_{\text{out}} R_1) + \sum_{w=0}^{4} C_w^{\text{out2}} \alpha_{l0}^{w0} i_l'(\mu_{\text{out}} R_1), \tag{A1c}$$

$$C_l^{\text{in2}} i_l'(\mu_2 R_2) = C_l^{\text{out2}} k_l'(\mu_{\text{out}} R_2) + \sum_{w=0}^{4} C_w^{\text{out1}} \alpha_{l0}^{*w0} i_l'(\mu_{\text{out}} R_2); \tag{A1d}$$

Then, using these truncated series ($N = 4$) in the expressions for $F_{1z\varphi}$ and $F_{2z\varphi}$, we obtain the same results as those shown in Section V, but we stress that the numerical calculation for the acceleration of the *test* body becomes very unstable for small values of β.

Appendix B: Exploring the test particle limit in our specific (idealized) situation

In this appendix we show what happens in our proposal when the radius, R_2, of the *test* body tends to zero while the density ρ_2 (and μ_2) remain constant. First, we did this numerically within the approach presented in Section II B and confirmed that there are no violations of the WEP when the *thin shell* condition in the *large* body ensues.

We implement two simplified models that provide more insight about this limit. In the first one, we take the chameleon field outside the *test* body to be that due to the *large* body alone (which is easily found) and thus we require only to compute the field inside the *test* body. In the second model, we assume *ab initio* that the *test* body is literally a *test point particle*, and thus, that it does not produce any back-reaction on the *large* body and the environment. Hence, we take the chameleon as generated solely by these two sources. That is, in this case the problem reduces to the usual one body problem (OBP) that has been studied in the past, and which corresponds to the static and spherically symmetric solution of the chameleon equation with one body surrounded by an environment.

So let us start analyzing the first of these two models that we call the simplified two body problem (STBP). Under the STBP we take the OBP solution in the outside region and inside the *large* body (see Appendix E for a review on the OBP solution). However, inside the *test* body we consider the solution that matches continuously on its boundary with the exterior field. In order to do this we take the most general regular solution of the differential equation in that region, which is given by

$$\varphi_{\text{in2}}(r', \phi', \theta') = \varphi(r', \phi', \theta') = \sum_{lm} C_{lm}^{in2} i_l(\mu_2 r') Y_{lm}(\theta', \phi') + \varphi_c^{\text{test body}} \qquad (r' \le R_2) \ , \qquad \text{(B1)}$$

where R_2 is the radius of the *test* body, and the primed spherical coordinates are taken with respect to a frame of reference centered at the origin of the *test* body. Like in the analysis of Section II B, inside the *test* body we consider only the MSBF's of the first type $i_l(.)$ which are regular at $r' = 0$ as opposed to the MSBF's of second type $k_l(.)$, which are regular at infinity. We have introduced the notation $\varphi_c^{\text{test body}} = \varphi_{\text{2min}}^{\text{in}}$, for the minimum of $V_{\text{eff}}(\varphi)$ inside the *test* body, and similarly, $\mu_2 = m_{\text{eff}}^{\text{test body}}$. In fact, the STBP that we analyze is *axially symmetric* (i.e. symmetric around the $z - axis$ that connects the centers of the two bodies as shown in Figure 2), thus, we need only the coefficients with $m = 0$ (the others vanish identically).

As we indicated, here we take the chameleon outside the *test* body to be well approximated by the exterior field of the OBP (see Appendix E):

$$\varphi^{\text{out}}(r) = C \frac{\exp\left[-\mu_{\text{out}} r\right]}{r} + \varphi_\infty \ , \qquad \text{(B2)}$$

where $\mu_{\text{out}} = m_{\text{eff}}^{\text{out}}$ is the effective mass of the chameleon associated with the environment, $\vec{r}' = \vec{r} - D\hat{z}$, D is the distance between the centers of the two bodies (see Figure 2) and C is a constant that is found when matching the exterior with the interior solution of the OBP (see Appendix E). Let us remind that in the STBP we are ignoring the effect of the *test* body on the exterior solution, thus, for the STBP we only require the exterior solution of the *large* body as if the *test* body were absent. The coefficients of the expansion in Eq. (B1) are found by matching this solution with the exterior solution Eq. (B2) at R_2. In order to do so we shall employ the following identity to rewrite $\varphi^{\text{out}}(r)$ in terms of the coordinate system centered at the *test* body:

$$\frac{\exp\left[-\mu_{\text{out}}|\vec{r}_2 - \vec{r}_1|\right]}{4\pi|\vec{r}_2 - \vec{r}_1|} = \mu_{\text{out}} \sum_{l=0}^{\infty} i_l(\mu_{\text{out}} r_2) k_l(\mu_{\text{out}} r_1) \times \sum_{m=-l}^{l} Y_{lm}(\theta_2, \phi_2) Y_{lm}^*(\theta_1, \phi_1),$$

as long as $r_2 < r_1$ and being $k_l(.)$ the MSBF of second type mentioned previously. In the current case $\vec{r}_1 = -D\hat{z}$, $\theta_1 = 0$, and $\vec{r}_2 = \vec{r}'$. As mentioned before only the terms with $m = 0$ contribute to the solution. The matching condition $\varphi_{\text{in2}}(R_2) = \varphi_{\text{out}}(R_2)$, leads to

$$C_{l0}^{\text{in2}} = \left[\frac{(\varphi_\infty - \varphi_c^{\text{tbody}})\delta_{l0}}{2l + 1} + C\mu_{\text{out}} i_l(\mu_{\text{out}} R_2) k_l(\mu_{\text{out}} D)\right] \times \frac{\sqrt{4\pi(2l + 1)}}{i_l(\mu_2 R_2)}. \qquad \text{(B3)}$$

Remarkably, even at this level of approximation, and despite considering the case of a universal coupling β, Eq. (B3), shows that the field inside the *test* body depends on the *test* body properties, like its size R_2 and composition [both μ_2 and φ_c^{tbody} depend on ρ_{tbody} according to Eqs. (11) and (12)].

As soon as ones considers *test* bodies as extended bodies, they can be an important source of the chameleon, and as such, their composition appears naturally in the detailed behaviour of the scalar field. It is important to emphasize that in this STBP, the approximation involves taking the scalar field outside the small body, and then using the varying value of that field on the small body's boundary to help determine the value of the field inside of it. That is done by enforcing continuity of the chameleon field on the small body's surface, but in the present approximation we cannot impose the continuity of the first derivative of the chameleon there. The reason is that as the field outside is fixed (i.e., it is not allowed to react to the small body) there are not enough undetermined coefficients in the resulting expansion (only the coefficients corresponding to the field in small body's interior) to impose the two conditions (continuity of the field and of its normal derivative). This discontinuity can produce serious consequences in the resulting force when the *test* body is of finite size. This is why we do not use this simplified model for that purpose. Nonetheless, in the limit where the small body goes to zero ($R_2 \to 0$) this drawback disappears, simply because the exterior field does not change over the infinitesimal region occupied by such point like body.

Now, we want precisely to consider this limit. First, the coefficient of the chameleon in spherical harmonics with $l = 0$ associated with the solution due to the *large* body behaves as follows

$$C_{00}^{\text{in}1} \sim \frac{\sqrt{4\pi}\mu_1(1 + \mu_{\text{out}}R_1)(\varphi_\infty - \varphi_{1\text{min}}^{\text{in}})\operatorname{csch}(\mu_1 R_1)}{\mu_{\text{out}} + \mu_1 \coth(\mu_1 R_1)}, \tag{B4a}$$

$$C_{00}^{\text{out}1} \sim \frac{\sqrt{4\pi}\exp[\mu_{\text{out}}R_1]\mu_{\text{out}}(\varphi_{1\text{min}}^{\text{in}} - \varphi_\infty)\{\mu_1 R_1 \cosh(\mu_1 R_1) - \sinh(\mu_1 R_1)\}}{\mu_1 \cosh(\mu_1 R_1) + \mu_{\text{out}} \sinh(\mu_1 R_1)}, \tag{B4b}$$

$$C_{00}^{\text{out}2} \sim 0. \tag{B4c}$$

By construction, the chameleon field inside the *large* body and outside both bodies does not depend on anything coming from the *test* body. On the other hand, the coefficient $C_{00}^{\text{in}2}$ of Eq. (B3) in the limit $R_2 \to 0$ becomes,

$$C_{00}^{\text{in}2} \sim \sqrt{4\pi}\left\{(\varphi_\infty - \varphi_{2\text{min}}^{\text{in}}) + \frac{\exp[\mu_{\text{out}}(R_1 - D)](\varphi_\infty - \varphi_{1\text{min}}^{\text{in}})[\sinh(\mu_1 R_1) - \mu_1 R_1 \cosh(\mu_1 R_1)]}{D[\mu_1 \cosh(\mu_1 R_1) + \mu_{\text{out}} \sinh(\mu_1 R_1)]}\right\}. \tag{B5}$$

So, the field $\varphi_{\text{in}2}(\vec{r'})$ when $R_2 \to 0$ becomes

$$\varphi_{\text{in}2} \sim \varphi_\infty + \frac{\exp[\mu_{\text{out}}(R_1 - D)](\varphi_\infty - \varphi_{1\text{min}}^{\text{in}})[\sinh(\mu_1 R_1) - \mu_1 R_1 \cosh(\mu_1 R_1)]}{D[\mu_1 \cosh(\mu_1 R_1) + \mu_{\text{out}} \sinh(\mu_1 R_1)]}; \tag{B6}$$

Thus, it follows from the above equations that in this limit the chameleon field does not depend on the test particle composition, and thus, there is no effective violation of the WEP.

Let us now consider a different simplification, where the *test* body is taken as a test point particle from the very beginning. This is what one usually finds in most of the literature. Since one takes the *test* body as test particle and the *large* body and the environment as spherical sources of different uniform densities, one takes the following distribution for the matter part, $T^m \approx -\rho = -\mathcal{M}_2\delta(z - D)\delta(x)\delta(y) - \rho_{\text{in}}^1\Theta(r - R) - \rho_{\text{out}}\tilde{\Theta}(r, R)$, where $\mathcal{M}_2$ is the mass of the *test* body, and the step function $\tilde{\Theta}(r, R)$ is defined to be unity for $R < r < \infty$ and zero otherwise. The distribution $\rho_{\text{out}}\tilde{\Theta}(r, R)$ allows one to describe the environment of density ρ_{out}.

Therefore from Eq. (37) we obtain

$$U_\varphi \approx \varphi_{\text{out}}(\vec{r})\frac{\beta\mathcal{M}_2}{M_{pl}} + \text{const.} \tag{B7}$$

where $\vec{r}$ corresponds to the location of the point-test particle, and the constant contains information about the bulk properties of the *large* body, the environment and the point-test particle, but it is independent of the location of the latter. Thus the only contribution for the force arises only from the term in the integral of Eq. (37) that is proportional to $\hat{\varphi}T^m$, which contains the information of the chameleon and the location of the *test* body.

In this way, the chameleon force on the point-test particle reads

$$\vec{F} = -\vec{\nabla} U_\varphi = -\frac{\beta \mathcal{M}_2}{M_{pl}} \vec{\nabla} \varphi_{\text{out}} \quad,$$

(B8)

again, this is to be evaluated at the location of the point-test particle. Henceforth, we recover the same expression considered in [1] for the chameleon force acting on a point test-particle.

Now, in this limit the solution for the chameleon is given by Eq. (B2), which is the exterior solution of the one body problem in spherical symmetry. In order to give an insight of the Eötvös parameter and the way it can be constrained when a *thin shell* exists, it is better to take the constant C of Eq. (B2) as written in the form Eq. (E3). As explained in Appendix E below, when there is a *thin shell* the exterior solution reads [cf. Eq. (E3) with $f(x) \approx 1$]

$$\varphi^{\text{out}}(r) \approx \varphi_\infty - \frac{3\beta \mathcal{M}}{4\pi M_{pl}} \frac{\Delta R}{R} \frac{\exp\left[-m_{\text{eff}}^{\text{out}}(r-R)\right]}{r} \quad.$$

(B9)

where $\mathcal{M}$ is the mass of the *large* body. For simplicity let us assume $r \sim R$ and $m_{\text{eff}}^{\text{out}}(r-R) \ll 1$. Thus

$$\varphi^{\text{out}}(r) \approx \varphi_\infty - \frac{3\beta}{4\pi M_{pl}} \frac{\Delta R}{R} \frac{\mathcal{M}}{r} \quad.$$

(B10)

Using this expression in (B8) the chameleon force on the point-test particle at distance $r = D$ turns out to be

$$\vec{F}_\varphi = -\hat{r} \frac{3\beta^2}{4\pi M_{pl}^2} \frac{\Delta R}{R} \frac{\mathcal{M}\mathcal{M}_2}{D^2} \quad,$$

(B11)

where $\hat{r}$ is the unit radial vector. Notice that the chameleon force is proportional to the gravitational force acting on the particle due to the *large* body

$$\vec{F}_g = -\hat{r} \frac{G\mathcal{M}_G \mathcal{M}_{G,2}}{D^2} \quad,$$

(B12)

where $\mathcal{M}_G$ and $\mathcal{M}_{G,2}$ are the *gravitational* masses of the *large* body and the point-test particle, respectively, as opposed to their *chameleon*-like masses (or "chameleon charges") $\mathcal{M}$ and $\mathcal{M}_2$. That is, the masses that couple to the chameleon force.

In this way, the magnitude of the acceleration of the point-test particle due to the *large* body is

$$a_2 = \frac{|\vec{F}_\varphi + \vec{F}_g|}{\mathcal{M}_{I,2}} = \frac{G\mathcal{M}_G}{D^2} \left(\frac{\mathcal{M}_{G,2}}{\mathcal{M}_{I,2}} + \frac{6\beta^2 \mathcal{M}_2 \mathcal{M}}{\mathcal{M}_{I,2}\mathcal{M}_G} \frac{\Delta R}{R} \right) \quad,$$

(B13)

where $\mathcal{M}_{I,2}$ is the *inertial* mass of the point-test particle and we used $G = 1/(8\pi M_{pl}^2)$.

If the coupling to the chameleon force is not universal then this acceleration reads

$$a_2 = \frac{G\mathcal{M}_G}{D^2} \left(\frac{\mathcal{M}_{G,2}}{\mathcal{M}_{I,2}} + \frac{6\beta_1\beta_2 \mathcal{M}_2 \mathcal{M}}{\mathcal{M}_{I,2}\mathcal{M}_G} \frac{\Delta R}{R} \right) \quad.$$

(B14)

where β_1 is the chameleon coupling to the large body.

A similar expression is obtained for the acceleration of a second point-test particle except that the masses $\mathcal{M}_2, \mathcal{M}_{G,2}$ and $\mathcal{M}_2^I$ of the first point-test particle are replaced by the masses $\mathcal{M}_3, \mathcal{M}_{G,3}$ and $\mathcal{M}_3^I$ of the second point-test particle, and similarly β_2 is replaced by β_3.

Therefore the relative acceleration of two "free-falling" point-test particles under the influence of both gravity and the chameleon due to the *large* body is

$$|a_2 - a_3| = \frac{G\mathcal{M}_G}{D^2} \left| \frac{\mathcal{M}_{G,2}}{\mathcal{M}_{I,2}} - \frac{\mathcal{M}_{G,3}}{\mathcal{M}_{I,3}} + \left(\frac{\beta_2 \mathcal{M}_2}{\mathcal{M}_{I,2}} - \frac{\beta_3 \mathcal{M}_3}{\mathcal{M}_{I,3}} \right) \frac{6\beta_1 \mathcal{M}}{\mathcal{M}_G} \frac{\Delta R}{R} \right| \quad.$$

(B15)

The Eötvös parameter is thus given by

$$\eta = \frac{2|a_2 - a_3|}{a_2 + a_3} = 2 \frac{\left| \frac{\mathcal{M}_{G,2}}{\mathcal{M}_{I,2}} - \frac{\mathcal{M}_{G,3}}{\mathcal{M}_{I,3}} + \left(\frac{\beta_2 \mathcal{M}_2}{\mathcal{M}_{I,2}} - \frac{\beta_3 \mathcal{M}_3}{\mathcal{M}_{I,3}} \right) \frac{6\beta_1 \mathcal{M}}{\mathcal{M}_G} \frac{\Delta R}{R} \right|}{\frac{\mathcal{M}_{G,2}}{\mathcal{M}_{I,2}} + \frac{\mathcal{M}_{G,3}}{\mathcal{M}_{I,3}} + \left(\frac{\beta_2 \mathcal{M}_2}{\mathcal{M}_{I,2}} + \frac{\beta_3 \mathcal{M}_3}{\mathcal{M}_{I,3}} \right) \frac{6\beta_1 \mathcal{M}}{\mathcal{M}_G} \frac{\Delta R}{R}} \quad.$$

(B16)

Taking $\beta_i = 0$ $(i = 1 - 3)$ we recover the usual expression of this parameter only due to gravity. On the other hand, for $\beta_i \neq 0$ but assuming that the inertial and gravitational masses are the same, we obtain the Eötvös parameter due to the chameleon solely:

$$\eta = \frac{2|a_2 - a_3|}{a_2 + a_3} = \frac{\Delta R}{R} \frac{\frac{6\beta_1 \mathcal{M}}{\mathcal{M}_G} \left| \frac{\beta_2 \mathcal{M}_2}{\mathcal{M}_{I,2}} - \frac{\beta_3 \mathcal{M}_3}{\mathcal{M}_{I,3}} \right|}{1 + \left(\frac{\beta_2 \mathcal{M}_2}{\mathcal{M}_{I,2}} + \frac{\beta_3 \mathcal{M}_3}{\mathcal{M}_{I,3}} \right) \frac{3\beta_1 \mathcal{M}}{\mathcal{M}_G} \frac{\Delta R}{R}} \ . \tag{B17}$$

This expression is used to stress the importance of the *thin shell* condition $\Delta R \ll R$. If the equality between the chameleon-like mass and the inertial mass holds exactly as well, then the relative acceleration between the two point-test particles is only due to the difference $|\beta_2 - \beta_3|$ may not strictly vanish. Thus, if such a difference is of order unity, then the observations $\eta \sim 10^{-13}$ (or $\eta \sim 10^{-11}$ if one takes into account only the effects produced by the local inhomogeneities of the matter near the torsion balance) can be satisfied provided $\Delta R / R$ is small enough. This is the chameleon mechanism at work for the point-particle limit. Moreover, if the couplings β_i are universal, then $\eta \equiv 0$ regardless of whether the *large* body is associated with a *thin shell* or not. As we stressed before, in the universal-coupling scenario we checked numerically that $\eta \to 0$ in our full model of Section II B as we reduced the size of the (extended) *test* body.

Summarizing, the standard assumption is that the *screening* effects produced by the chameleon behaviour, effectively suppress the dependency of η on the the couplings β_i in models where this parameter is not universal. Nonetheless, as we have shown here such supposition seems to work only for the true point-particle limit of *test* bodies, but not at the more precise level of the current analysis which is the relevant one for consideration of actual experimental test, where the *test* bodies are not just point particles, but small bodies of finite size.

Appendix C: Composition dependence of the effective force

Let us consider the expressions for the terms $F_{1z\varphi}$ and $F_{2z\varphi}$ of Section IV, and replace the explicit series expansions for the chameleon field found in Section II B. The result is

$$
\begin{aligned}
F_{1z\varphi} &= \int_0^{R_2} \int_0^\pi \int_0^{2\pi} \left[\frac{(n+1)}{2} \frac{\rho_2 \beta}{M_{pl}} \right] \left[\sum_l \frac{\partial C_{l0}^{\text{in2}}}{\partial D} i_l(\mu_2 r') Y_{l0}(\theta', \phi') \right] r'^2 \sin(\theta') d\phi' d\theta' dr' \\
&+ \int_0^{R_1} \int_0^\pi \int_0^{2\pi} \left[\frac{(n+1)}{2} \frac{\rho_1 \beta}{M_{pl}} \right] \left[\sum_l \frac{\partial C_{l0}^{\text{in1}}}{\partial D} i_l(\mu_1 r) Y_{l0}(\theta, \phi) \right] r^2 \sin(\theta) d\phi d\theta dr \\
&+ \int_{R_1}^\infty \int_0^\pi \int_0^{2\pi} \left[\frac{(n+1)}{2} \frac{\rho_{\text{out}} \beta}{M_{pl}} \right] \left[\sum_l \frac{\partial C_{l0}^{\text{out1}}}{\partial D} k_l(\mu_{\text{out}} r) Y_{l0}(\theta, \phi) \right] r^2 \sin(\theta) d\phi d\theta dr \\
&+ \int_{R_1}^D \int_0^\pi \int_0^{2\pi} \left[\frac{(n+1)}{2} \frac{\rho_{\text{out}} \beta}{M_{pl}} \right] \\
&\times \left[\sum_l \sum_{w=0}^N \left\{ \frac{\partial C_{l0}^{\text{out2}}}{\partial D} \alpha_{w0}^{l0} + C_{l0}^{\text{out2}} \frac{\partial \alpha_{w0}^{l0}}{\partial D} \right\} i_w(\mu_{\text{out}} r) Y_{w0}(\theta, \phi) \right] r^2 \sin(\theta) d\phi d\theta dr \\
&+ \int_D^\infty \int_0^\pi \int_0^{2\pi} \left[\frac{(n+1)}{2} \frac{\rho_{\text{out}} \beta}{M_{pl}} \right] \\
&\times \left[\sum_l \sum_{w=0}^N \left\{ \frac{\partial C_{l0}^{\text{out2}}}{\partial D} \hat{\alpha}_{w0}^{l0} + C_{l0}^{\text{out2}} \frac{\partial \hat{\alpha}_{w0}^{l0}}{\partial D} \right\} k_w(\mu_{\text{out}} r) Y_{w0}(\theta, \phi) \right] r^2 \sin(\theta) d\phi d\theta dr \\
&- \int_0^{R_2} \int_0^\pi \int_0^{2\pi} \left[\frac{(n+1)}{2} \frac{\rho_{\text{out}} \beta}{M_{pl}} \right] \\
&\times \left[\sum_l \sum_{w=0}^N \left\{ \frac{\partial C_{l0}^{\text{out1}}}{\partial D} \alpha_{w0}^{*l0} + C_{l0}^{\text{out1}} \frac{\partial \alpha_{w0}^{*l0}}{\partial D} \right\} i_w(\mu_{\text{out}} r') Y_{w0}(\theta', \phi') \right] r'^2 \sin(\theta') d\phi' d\theta' dr',
\end{aligned}
$$

$$\tag{C1}$$

where

$$\hat{\alpha}_{vw}^{lm} = (-1)^{m+v}(2v+1) \sum_{p=|l-v|}^{|l+v|} (2p+1) \left[\frac{(l+m)!(v+w)!(p-m-w)!}{(l-m)!(v-w)!(p+m+w)!} \right]^{1/2}$$
$$\times \begin{bmatrix} l & v & p \\ 0 & 0 & 0 \end{bmatrix} \begin{bmatrix} l & v & p \\ m & w & -m-w \end{bmatrix} i_p(\mu_{\text{out}}|D|) Y_{p(m-w)}(\theta_D, \phi_D). \tag{C2}$$

The integral $\int_0^{2\pi} \int_0^{\pi} Y_{l0}(\theta_j, \phi_j) \sin(\theta_j) d\theta_j d\phi_j$, which appears inside all the terms in the expression for $F_{1z\varphi}$, vanishes when $l \neq 0$. Meanwhile, integrals like $\int_0^R i_l(mr)r^2 dr$ and $\int_R^{\infty} k_l(mr)r^2 dr$, and the derivatives $\partial C_{l0}^{\text{in(out)}\,1(2)}/\partial D$ converge to finite values for all values of l. Consequently, the only contribution to the first three integrals of Eq. (C1) is the term with $l = 0$, while the last integrals of Eq. (C1) only have no null terms for $w = 0$ being l arbitrary in this case. In this way, we obtain for the linear term of the force:

$$\begin{aligned}
F_{1z\varphi} =\ & \left[\frac{(n+1)}{2} \frac{\rho_2 \beta}{M_{pl}} \right] 2\sqrt{\pi} \frac{\partial C_{00}^{\text{in2}}}{\partial D} \left[\frac{\mu_2 R_2 \cosh(\mu_2 R_2) - \sinh(\mu_2 R_2)}{\mu_2^3} \right] \\
& + \left[\frac{(n+1)}{2} \frac{\rho_1 \beta}{M_{pl}} \right] 2\sqrt{\pi} \left[\frac{\mu_1 R_1 \cosh(\mu_1 R_1) - \sinh(\mu_1 R_1)}{\mu_1^3} \right] \frac{\partial C_{00}^{\text{in1}}}{\partial D} \\
& + \left[\frac{(n+1)}{2} \frac{\rho_{\text{out}} \beta}{M_{pl}} \right] 2\sqrt{\pi} \frac{\partial C_{00}^{\text{out1}}}{\partial D} \left[\frac{\exp[-\mu_{\text{out}} R_1](1 + R_1)}{\mu_{\text{out}}^3} \right] \\
& + \left[\frac{(n+1)}{2} \frac{\rho_{\text{out}} \beta}{M_{pl}} \right] 2\sqrt{\pi} \sum_l \left\{ \frac{\partial C_{l0}^{\text{out2}}}{\partial D} \alpha_{00}^{l0} + C_{l0}^{\text{out2}} \frac{\partial \alpha_{00}^{l0}}{\partial D} \right\} \\
& \times \left[\frac{-R_1 \cosh(\mu_{\text{out}} R_1) + D \cosh(\mu_{\text{out}} D)}{\mu_{\text{out}}^2} + \frac{\sinh(\mu_{\text{out}} R_1) - \sinh(\mu_{\text{out}} D)}{\mu_{\text{out}}^3} \right] \\
& + \left[\frac{(n+1)}{2} \frac{\rho_{\text{out}} \beta}{M_{pl}} \right] 2\sqrt{\pi} \sum_l \left\{ \frac{\partial C_{l0}^{\text{out2}}}{\partial D} \hat{\alpha}_{00}^{l0} + \frac{\partial \hat{\alpha}_{00}^{l0}}{\partial D} C_{l0}^{\text{out2}} \right\} \frac{\exp[-\mu_{\text{out}} R_1](1 + \mu_{\text{out}} R_1)}{\mu_{\text{out}}^3} \\
& - \left[\frac{(n+1)}{2} \frac{\rho_{\text{out}} \beta}{M_{pl}} \right] 2\sqrt{\pi} \\
& \times \sum_l \left\{ \frac{\partial C_{l0}^{\text{out1}}}{\partial D} \alpha_{00}^{*l0} + \frac{\partial \alpha_{00}^{*l0}}{\partial D} C_{l0}^{\text{out1}} \right\} \left[\frac{\mu_{\text{out}} R_2 \cosh(\mu_{\text{out}} R_2) - \sinh(\mu_{\text{out}} R_2)}{\mu_{\text{out}}^3} \right].
\end{aligned} \tag{C3}$$

The quadratic term can be expressed as:

$$
\begin{aligned}
F_{2z\varphi} = {} & -\int_{V_2}\left[\frac{(n+2)}{4}\mu_2^2\right]\frac{\partial}{\partial D}\left[\sum_w\sum_l C_{l0}^{\text{in}2}i_l(\mu_2 r')Y_{l0}(\theta',\varphi')C_{w0}^{\text{in}2}i_w(\mu_2 r')Y_{w0}(\theta',\phi')\right]r'^2\sin(\theta')dV_2\\
& -\int_{V_1}\left[\frac{(n+2)}{4}\mu_1^2\right]\frac{\partial}{\partial D}\left[\sum_w\sum_l C_{l0}^{\text{in}1}i_l(\mu_1 r)Y_{l0}(\theta,\phi)C_{w0}^{\text{in}1}i_l(\mu_1 r)Y_{w0}(\theta,\phi)\right]r^2\sin(\theta)dV_1\\
& -\int_{R_1}^{\infty}\int_0^{\pi}\int_0^{2\pi}\left[\frac{(n+2)}{4}\mu_{\text{out}}^2\right]\frac{\partial}{\partial D}\left[\sum_v\sum_l C_{l0}^{\text{out}1}k_l(\mu_{\text{out}} r)Y_{l0}(\theta,\phi)C_{v0}^{\text{out}1}k_v(\mu_{\text{out}} r)Y_{v0}(\theta,\phi)\right]r^2\sin(\theta)d\phi d\theta dr\\
& -\int_{R_1}^{D}\int_0^{\pi}\int_0^{2\pi}\left[\frac{(n+2)}{4}\mu_{\text{out}}^2\right]\\
& \times\frac{\partial}{\partial D}\left[\sum_v\sum_l C_{l0}^{\text{out}1}k_l(\mu_{\text{out}} r)Y_{l0}(\theta,\phi)C_{v0}^{\text{out}2}\sum_w^N\alpha_{w0}^{v0}i_w(\mu_{\text{out}} r)Y_{w0}(\theta,\phi)\right]r^2\sin(\theta)d\phi d\theta dr\\
& -\int_D^{\infty}\int_0^{\pi}\int_0^{2\pi}\left[\frac{(n+2)}{4}\mu_{\text{out}}^2\right]\\
& \times\frac{\partial}{\partial D}\left[\sum_v\sum_l C_{l0}^{\text{out}1}k_l(\mu_{\text{out}} r)Y_{l0}(\theta,\phi)C_{v0}^{\text{out}2}\sum_w^N\hat\alpha_{w0}^{v0}k_w(\mu_{\text{out}} r)Y_{w0}(\theta,\phi)\right]r^2\sin(\theta)d\phi d\theta dr\\
& -\int_{R_1}^{D}\int_0^{\pi}\int_0^{2\pi}\left[\frac{(n+2)}{4}\mu_{\text{out}}^2\right]\\
& \times\frac{\partial}{\partial D}\left[\sum_l C_{l0}^{\text{out}2}\sum_u^N\alpha_{u0}^{l0}i_u(\mu_{\text{out}} r)Y_{u0}(\theta,\varphi)\sum_v C_{v0}^{\text{out}2}\sum_w^N\alpha_{w0}^{v0}i_w(\mu_{\text{out}} r)Y_{w0}(\theta,\phi)\right]r^2\sin(\theta)d\phi d\theta dr\\
& -\int_D^{\infty}\int_0^{\pi}\int_0^{2\pi}\left[\frac{(n+2)}{4}\mu_{\text{out}}^2\right]\\
& \times\frac{\partial}{\partial D}\left[\sum_l C_{l0}^{\text{out}2}\sum_u^N\hat\alpha_{u0}^{l0}k_u(\mu_{\text{out}} r)Y_{u0}(\theta,\phi)\sum_v C_{v0}^{\text{out}2}\sum_w^N\hat\alpha_{w0}^{v0}k_w(\mu_{\text{out}} r)Y_{w0}(\theta,\phi)\right]r^2\sin(\theta)d\phi d\theta dr\\
& +\int_0^{R_2}\int_0^{\pi}\int_0^{2\pi}\left[\frac{(n+2)}{4}\mu_{\text{out}}^2\right]\\
& \times\frac{\partial}{\partial D}\left[\sum_l C_{l0}^{\text{out}1}\sum_u^N\alpha_{u0}^{*l0}i_u(\mu_{\text{out}} r')Y_{u0}(\theta',\phi')\sum_v C_{v0}^{\text{out}1}\sum_w^N\alpha_{w0}^{*v0}i_w(\mu_{\text{out}} r')Y_{w0}(\theta',\phi')\right]r^2\sin(\theta')d\phi' d\theta' dr'
\end{aligned}
$$

$$\tag{C4}$$

The angular integral that appears inside all the terms in the expression for $F_{2z\varphi}$ is,

$$
\int_0^{2\pi}\int_0^{\pi}Y_{l0}(\theta_j,\phi_j)Y_{k0}(\theta_j,\phi_j)\sin(\theta_j)d\theta_j d\phi_j = \frac{4\pi\sqrt{(2l+1)(2k+1)}k!}{4\pi(2k+1)k!}\delta_{kl} = \delta_{kl}.
$$

Therefore,

$$F_{2z\varphi} = -\sum_l \frac{(n+2)}{4}\mu_2^2 \frac{\partial}{\partial D}\left[C_{l0}^{in2}C_{l0}^{in2}\right]\frac{R_2^3}{2}\left\{[i_l(\mu_2 R_2)]^2 - i_{l-1}(\mu_2 R_2)i_{l+1}(\mu_2 R_2)\right\}$$

$$-\sum_l \frac{(n+2)}{4}\mu_1^2 \frac{\partial}{\partial D}\left[C_{l0}^{in1}C_{l0}^{in1}\right]\frac{R_1^3}{2}\left\{[i_l(\mu_1 R_1)]^2 - i_{l-1}(\mu_1 R_1)i_{l+1}(\mu_1 R_1)\right\}$$

$$-\sum_l \frac{(n+2)}{4}\mu_{out}^2 \frac{\partial}{\partial D}\left[C_{l0}^{out1}C_{l0}^{out1}\right]\frac{R_1^3}{2}\left\{[k_l(\mu_{out} R_1)]^2 - k_{l-1}(\mu_{out} R_1)k_{l+1}(\mu_{out} R_1)\right\}$$

$$-\sum_w \sum_l^N \frac{(n+2)}{4}\mu_{out}^2 \frac{\partial}{\partial D}\left[C_{w0}^{out2}C_{l0}^{out1}\alpha_{l0}^{w0}\right]\left\{Q_2(l,D) - Q_2(l,R_1)\right\}$$

$$-\sum_w \sum_l^N \frac{(n+2)}{4}\mu_{out}^2 \frac{\partial}{\partial D}\left[C_{w0}^{out2}C_{l0}^{out1}\hat{\alpha}_{l0}^{w0}\right]\frac{D^3}{2}\left\{[k_l(\mu_{out} D)]^2 - k_{l-1}(\mu_{out} D)k_{l+1}(\mu_{out} D)\right\}$$

$$-\sum_l \sum_w \sum_v^N \frac{(n+2)}{4}\mu_{out}^2 \frac{\partial}{\partial D}\left[C_{w0}^{out2}C_{l0}^{out2}\alpha_{v0}^{w0}\alpha_{v0}^{l0}\right]\left\{Q_3(v,D) - Q_3(v,R_1)\right\}$$

$$-\sum_w \sum_l \sum_v^N \frac{(n+2)}{4}\mu_{out}^2 \frac{\partial}{\partial D}\left[C_{w0}^{out2}C_{l0}^{out2}\hat{\alpha}_{v0}^{w0}\hat{\alpha}_{v0}^{l0}\right]$$

$$\times \frac{D^3}{2}\left\{[k_v(\mu_{out} D)]^2 - k_{v-1}(\mu_{out} D)k_{v+1}(\mu_{out} D)\right\}$$

$$+\sum_w \sum_l \sum_v^N \frac{(n+2)}{4}\mu_{out}^2 \frac{\partial}{\partial D}\left[C_{w0}^{out1}C_{l0}^{out1}\alpha_{v0}^{*w0}\alpha_{v0}^{*l0}\right]$$

$$\times \frac{R_2^3}{2}\left\{[i_v(\mu_{out} R_2)]^2 - i_{v-1}(\mu_{out} R_2)i_{v+1}(\mu_{out} R_2)\right\} , \tag{C5}$$

where

$$Q_2(l,r) = -\frac{2l+1}{4\mu_{out}^3} + \frac{r^3}{2}\left\{i_l(\mu_{out}r)k_l(\mu_{out}r) + i_{l-1}(\mu_{out}r)k_{l-1}(\mu_{out}r)\right\},$$

$$Q_3(v,r) = \frac{r^3}{2}\left\{\left[i_v(\mu_{out}r)\right]^2 - i_{v-1}(\mu_{out}r)i_{v+1}(\mu_{out}r)\right\}.$$

As we underlined at the end of Section IV, the expressions for $F_{1z\varphi}$ and $F_{2z\varphi}$ show the explicit dependence of the chameleon mediated force with the composition and size of the *test* body through the quantities ρ_2, C_{l0}^{in2}, C_{l0}^{in1}, C_{l0}^{out2}, C_{l0}^{out1} and their derivatives.

Appendix D: The two body problem solution for the chameleon with the metal encasing

Figure 8 represents a sketch of the two body problem with a metal encasing around the *test* body. As one can see, both, the atmosphere inside the encasing and metal encasing itself, can be described under the same coordinate system that describes the *test* body, that is, O'. Accordingly, the solution for the chameleon field is given by,

$$\varphi = \begin{cases} \varphi_{in1} = \sum_{lm} C_{lm}^{in1} i_l(\mu_1 r)Y_{lm}(\theta,\phi) + \varphi_{1min}^{in} & (r \leq R_1) \\ \varphi_{out} = \sum_{lm} C_{lm}^{out1} k_l(\mu_{out} r)Y_{lm}(\theta,\phi) + C_{lm}^{out2} k_l(\mu_{out} r')Y_{lm}(\theta',\phi') + \varphi_{\infty} & \text{(exterior solution)} \\ \varphi_{in2} = \sum_{lm} C_{lm}^{in2} i_l(\mu_2 r')Y_{lm}(\theta',\phi') + \varphi_{2min}^{in} & (r' \leq R_2) \\ \varphi_{vacuum} = \sum_{lm} C_{lm}^{vac1} i_l(\mu_{vac} r')Y_{lm}(\theta',\phi') + C_{lm}^{vac2} k_l(\mu_{vac} r')Y_{lm}(\theta',\phi') + \varphi_{min}^{vac} & (R_2 \leq r' \leq R_{vac}) \\ \varphi_{encasing} = \sum_{lm} C_{lm}^{enc1} i_l(\mu_{enc} r')Y_{lm}(\theta',\phi') + C_{lm}^{enc2} k_l(\mu_{enc} r')Y_{lm}(\theta',\phi') + \varphi_{min}^{enc} & (R_{vac} \leq r' \leq R_{enc}) \end{cases} \tag{D1}$$
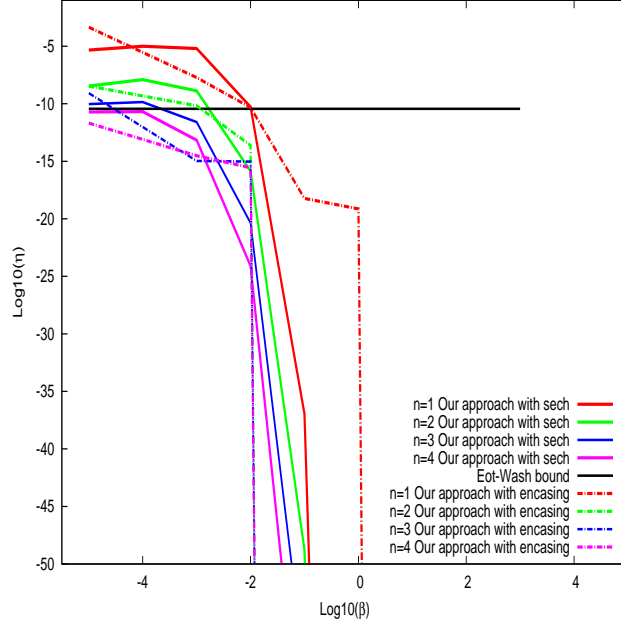
Figure 15: The Eötvös parameter η (in $\log_{10}$ scale) as a function of the parameter β (in $\log_{10}$ scale) including the metal encasing of the vacuum chamber as shown in Fig. 8 for different positive values of n and $M = 2.4$ meV. Here we assume that both the density of the environment surrounding the Earth (and of course, the hill) and inside the vacuum chamber are $\rho_{\text{out}} = 10^{-7}$g cm^{-3}. We compare our predictions considering the metal encasing in the calculations with those of ours too, but where the effect of the metal encasing is modeled multiplying a factor sech($2m_{\text{shell}}$d) to the predictions.

where the "new" magnitudes $\mu_{\text{vac}} = m_{\text{eff}}^{\text{vacuum}}$, $\mu_{\text{enc}} = m_{\text{eff}}^{\text{encasing}}$, $\varphi_{\text{min}}^{\text{vac}}$ and $\varphi_{\text{min}}^{\text{enc}}$ represents the value of the chameleon field that minimizes the effective potential in each region, and $R_{\text{vac}}, R_{\text{enc}}$ are the radii of the vacuum chamber and the metal encasing, respectively. Similarly to the proposal in section II B, the coefficients C_{lm} of Eq. (D1) are calculated using the following continuity conditions for the field and its derivative at the boundaries of the different regions:

$$\varphi_{\text{in1}}(r = R_1) = \varphi_{\text{out}}(r = R_1), \qquad \partial_r \varphi_{\text{in1}}(r = R_1) = \partial_r \varphi_{\text{out}}(r = R_1),$$

$$\varphi_{\text{in2}}(r' = R_2) = \varphi_{\text{vacuum}}(r' = R_2), \qquad \partial_{r'} \varphi_{\text{in2}}(r' = R_2) = \partial_{r'} \varphi_{\text{vacuum}}(r' = R_2);$$

$$\varphi_{\text{vacuum}}(r' = R_{\text{vac}}) = \varphi_{\text{encasing}}(r' = R_{\text{vac}}), \qquad \partial_{r'} \varphi_{\text{vacuum}}(r' = R_{\text{vac}}) = \partial_{r'} \varphi_{\text{encasing}}(r' = R_{\text{vac}});$$

$$\varphi_{\text{encasing}}(r' = R_{\text{enc}}) = \varphi_{\text{out}}(r' = R_{\text{enc}}), \qquad \partial_{r'} \varphi_{\text{encasing}}(r' = R_{\text{enc}}) = \partial_{r'} \varphi_{\text{out}}(r' = R_{\text{enc}});$$

Once the C_{lm} coefficients are obtained, both the energy associated with the total EMT, and then, the chameleon force; could be compute in a very similar way that has been explained in section IV and appendix C but adding the new regions.

We compare the predictions for the Eötvös parameter obtained under this scheme, with those obtained previously in section V (for the Eöt-Wash Torsion Balance Experiments) but applying the Yukawa type suppression sech($2m_{\text{shell}}$d) to these last predictions. We show these results in Fig.15. For $n = 1$ and $\beta > 10^{-2}$, the approach including the metal encasing presents an underestimation of the parameters compared to those obtained with the Yukawa suppression; while for $\beta \leq 10^{-2}$, it is just the opposite with the exception of $\beta = 10^{-5}$. For other the cases, where $n > 1$, it is found that in the majority of the analyzed cases there is an underestimation in the scheme that considers the metal encasing against the scheme where the hyperbolic secant is applied. Beyond all these differences, it can be observed that both schemes have a very similar behaviour. For large values of β, the suppression due to the metal encasing is very large but becoming small for small values of β.

Appendix E: The one body problem solution for the chameleon

The quadratic approximation of the potential which consist in assuming $V_{\text{eff}}(\varphi) = \frac{m_{\text{eff}}^2}{2}(\varphi - \varphi_{\min})^2 + V_{\text{eff}}(\varphi_{\min})$, is valid when φ is not too far from φ_{min}. Later, in this appendix, we discuss the situations where this approximation is not a sufficiently good one. This is the approximation that we have used throughout this paper. For the one body problem (spherical symmetry) we present the analytical solution below.

- The interior solution ($r < R$) can be expressed:

$$\varphi^{\text{in}}(r) = \frac{(\varphi_0 - \varphi_c)\sinh(m_{\text{eff}}^{\text{in}} r)}{m_{\text{eff}}^{\text{in}} r} + \varphi_c \qquad (r \le R) \ , \tag{E1}$$

where $\varphi_c := \varphi_{\min}^{\text{in}}$ and the value of the scalar field at the origin is given by

$$\varphi_0 = \varphi_c + \frac{(\varphi_\infty - \varphi_c)\left[1 + m_{\text{eff}}^{\text{out}} R\right]}{\frac{m_{\text{eff}}^{\text{out}} R}{x}\sinh(x) + \cosh(x)},$$

with $x := m_{\text{eff}}^{\text{in}} R$.

- The exterior solution ($r > R$) is

$$\varphi^{\text{out}}(r) = C\frac{\exp\left[-m_{\text{eff}}^{\text{out}} r\right]}{r} + \varphi_\infty \qquad (r \ge R) \ , \tag{E2}$$

where

$$C = -\frac{3\beta\mathcal{M}}{4\pi M_{pl}}\frac{\Delta R}{R}\exp\left[m_{\text{eff}}^{\text{out}} R\right]f(x) \ , \tag{E3}$$

and

$$\frac{\Delta R}{R} = -\frac{4\pi M_{pl}R(\varphi_c - \varphi_\infty)}{3\beta\mathcal{M}} = -\frac{(\varphi_c - \varphi_\infty)}{6\beta M_{pl}\Phi_N} \ , \tag{E4}$$

$$f(x) := \frac{\left[\cosh(x) - \frac{\sinh(x)}{x}\right]}{\frac{m_{\text{eff}}^{\text{out}} R}{x}\sinh(x) + \cosh(x)} \ . \tag{E5}$$

$\frac{\Delta R}{R}$ is the so called *thin-shell parameter* introduced in [1], $\mathcal{M}$ and $\Phi_N = \frac{\mathcal{M}}{8\pi M_{pl}^2 R}$ are the mass and the Newtonian potential at the surface of the body, respectively. These solutions are found by demanding the following requirements: i) regularity condition at $r = 0$, i.e., $\varphi^{\text{in}}(0) = \varphi_0$, ii) continuity and differentiability at $r = R$, iii) the asymptotic condition $\varphi^{\text{out}}(r \to \infty) = \varphi_{\min}^{\text{out}} = \varphi_\infty$.

The so called *thin-shell* effect appears when $1 \ll m_{\text{eff}}^{\text{in}} R$. So, under this kind of regime the approximate expressions for the field inside and outside the body are:

$$\varphi^{\text{in}}(r) \approx \frac{2(\varphi_\infty - \varphi_c)\exp\left[-R m_{\text{eff}}^{\text{in}}\right]\sinh(m_{\text{eff}}^{\text{in}} r)}{m_{\text{eff}}^{\text{in}} r} + \varphi_c \qquad (r \le R) \ , \tag{E6}$$

$$\varphi^{\text{out}}(r) \approx R(\varphi_c - \varphi_\infty)\frac{\exp\left[-m_{\text{eff}}^{\text{out}}(r - R)\right]}{r} + \varphi_\infty \qquad (r \ge R) \ . \tag{E7}$$

Note that due to the exponential factor, the r dependence of $\varphi^{\text{in}}(r)$ is strongly suppressed in regions well inside the body (i.e. $r \ll R$; where $\varphi^{\text{in}}(r) \approx \varphi_c$), and it is only within a *thin shell* of size ΔR, which is near the surface of the body, that the field grows exponentially to match the exterior solution $\varphi^{\text{out}}(r)$. In addition, when $1 \ll x$ one verifies that $f(x) \approx 1$ when the density contrast between the body and the environment is high. This is the essence of the "chameleon effect": the *screening* effect that makes the chameleon behave like the electric potential within a conductor.

There is however what is called the *thin shell* approximation. This approximation consists in considering the following solutions in three regions [25]

---

[25] In [1] (Paper II), R_S is denoted R_{roll}.

$$\varphi = \begin{cases} \varphi_c := \varphi_{\min}^{\text{in}} & 0 \le r \le R_{\text{S}} \\ \\ \varphi_s(r) & R_{\text{S}} \le r \le R_{\text{S}} + \Delta R = R \\ \\ \varphi_{\text{thin}}^{\text{out}}(r) & R \le r \end{cases} \qquad (\text{E8})$$

So the interior solution is divided in two parts: one associated to the "electric conductor" behaviour of the chameleon φ_c where the field is almost constant and at the minimum of the potential, and another one corresponding to the *thin shell* region $\varphi_s(r)$ where the gradients are "high" and the field start interpolating to the exterior solution $\varphi_{\text{thin}}^{\text{out}}(r)$ which is supposed to be close to the minimum of the exterior effective potential. In this approximation the chameleon solutions φ_s and $\varphi_{\text{thin}}^{\text{out}}(r)$ satisfy the corresponding approximate equations:

$$\nabla^2 \varphi_s = \frac{\partial V_{\text{eff}}}{\partial \varphi} \approx \frac{\beta}{M_{pl}} \rho^{\text{in}} \ , \qquad (\text{E9})$$

$$\nabla^2 \varphi_{\text{thin}}^{\text{out}} = \frac{\partial V_{\text{eff}}}{\partial \varphi} \approx m_{\text{eff}}^{2\,\text{out}} \left(\varphi_{\text{thin}}^{\text{out}} - \varphi_\infty \right) \ , \qquad (\text{E10})$$

where $\varphi_\infty := \varphi_{\min}^{\text{out}}$.

The solutions of these two equations are, respectively

$$\varphi_s(r) = \frac{1}{M_{pl}} \left[\frac{\beta \rho^{\text{in}} r^2}{6} + \frac{A}{r} + B \right] \qquad (R_{\text{S}} \le r \le R) \ , \qquad (\text{E11})$$

$$\varphi_{\text{thin}}^{\text{out}}(r) = C_{\text{thin}}^{\text{out}} \frac{e^{-m_{\text{eff}}^{\text{out}} r}}{r} + \varphi_\infty \qquad (R \le r) \qquad (\text{E12})$$

where $A, B, C_{\text{thin}}^{\text{out}}$ are integration constants.

When matching the thin shell solution continuously and smoothly with φ_c ar R_{S} we find

$$\varphi_s(r) = \frac{\beta \rho^{\text{in}}}{6 M_{pl}} \left(r^2 + \frac{2 R_{\text{S}}^3}{r} \right) - \frac{\beta \rho^{\text{in}}}{2 M_{pl}} R_{\text{S}}^2 + \varphi_c \qquad (R_{\text{S}} \le r \le R) \qquad (\text{E13})$$

On the other hand, when matching $\varphi_s(r)$ continuously and smoothly with $\varphi_{\text{thin}}^{\text{out}}(r)$ at the border of the body $r = R$ one finds that the constants $C_{\text{thin}}^{\text{out}}$ and R_{S} are obtained from the following algebraic equations:

$$C_{\text{thin}}^{\text{out}} = e^{m_{\text{eff}}^{\text{out}} R} \left\{ (\varphi_c - \varphi_\infty) R + \frac{\beta \rho^{\text{in}} R^3}{6 M_{pl}} \left[1 - 3 \frac{R_{\text{S}}^2}{R^2} + 2 \frac{R_{\text{S}}^3}{R^3} \right] \right\} \ ,$$

$$-\frac{C_{\text{thin}}^{\text{out}}}{R^2} e^{-m_{\text{eff}}^{\text{out}} R} \left(R m_{\text{eff}}^{\text{out}} + 1 \right) = \frac{\beta \rho^{\text{in}} R}{3 M_{pl}} \left(1 - \frac{R_{\text{S}}^3}{R^3} \right)$$

The most interesting approximation for these constants and thus, for the solution itself is when assuming that the thin shell parameter $\Delta R/R = 1 - R_{\text{S}}/R$ is small $\Delta R/R \ll 1$. Moreover, if one assumes $m_{\text{eff}}^{\text{out}} R \ll 1$ (i.e. the Compton wave length of the chameleon in the exterior region is large compared to the body's size) one finds

$$\frac{\Delta R}{R} \approx -\frac{(\varphi_c - \varphi_\infty)}{6 \beta M_{pl} \mathcal{M} G/R} = -\frac{(\varphi_c - \varphi_\infty)}{6 \beta M_{pl} \Phi_N} \ , \qquad (\text{E14})$$

where $\Phi_N = G\mathcal{M}/R$ stands for the Newtonian potential at the surface of the body and $\mathcal{M} = 4\pi \rho^{\text{in}} R^3/3$ is the mass of the body.

We also find the approximate expression,

$$C_{\text{thin}}^{\text{out}} \approx R (\varphi_c - \varphi_\infty) = -\frac{3}{4\pi} \frac{\beta \mathcal{M}}{M_{pl}} \frac{\Delta R}{R} \ . \qquad (\text{E15})$$

In this way, we find the approximate solution

$$\varphi_{\text{thin}}^{\text{out}}(r) \approx -\frac{\beta}{4\pi M_{pl}} \frac{3\Delta R}{R} \mathcal{M} \frac{e^{-m_{\text{eff}}^{\text{out}} r}}{r} + \varphi_\infty \qquad (R \le r) \qquad (\text{E16})$$

We appreciate the way the r dependence of the exterior solution is suppressed by the thin shell parameter.

One could be also interested in the *thick shell* solution corresponding to $R_S \to 0$ or equivalently, $\Delta R \approx R$. In this case the most internal region $0 \leq r \leq R_S$ "disappears" and the solution $\varphi_c \to \varphi_0$, i.e., it is the value of the field at $r = 0$. So there is only one interior solution $\varphi_s(r) \to \varphi_{\text{in}}(r)$ and one exterior one $\varphi_{\text{thick}}^{\text{out}}(r)$, provided respectively by

$$\varphi_{\text{in}}(r) = \frac{\beta \rho^{\text{in}}}{6 M_{pl}} r^2 + \varphi_0 \qquad (0 \leq r \leq R) \ , \tag{E17}$$

$$\varphi_{\text{thick}}^{\text{out}}(r) = C_{\text{thick}}^{\text{out}} \frac{e^{-m_{\text{eff}}^{\text{out}} r}}{r} + \varphi_\infty \qquad (R \leq r) \ . \tag{E18}$$

When matching continuously and smoothly both solutions at $r = R$ we determine the values of the constants φ_0 and $C_{\text{thick}}^{\text{out}}$. These are obtained from

$$C_{\text{thick}}^{\text{out}} = R e^{m_{\text{eff}}^{\text{out}} R} \left\{ (\varphi_0 - \varphi_\infty) + \frac{\beta \rho^{\text{in}} R^2}{6 M_{pl}} \right\} \ , \tag{E19}$$

$$-\frac{C_{\text{thick}}^{\text{out}}}{R^2} e^{-m_{\text{eff}}^{\text{out}} R} \left(R m_{\text{eff}}^{\text{out}} + 1 \right) = \frac{\beta \rho^{\text{in}} R}{3 M_{pl}} \ . \tag{E20}$$

Again, when assuming $m_{\text{eff}}^{\text{out}} R \ll 1$ one finds

$$C_{\text{thick}}^{\text{out}} \approx R \left\{ (\varphi_0 - \varphi_\infty) + \frac{\beta \rho^{\text{in}} R^2}{6 M_{pl}} \right\} \ , \tag{E21}$$

$$C_{\text{thick}}^{\text{out}} \approx -\frac{\beta \rho^{\text{in}} R^3}{3 M_{pl}} \ . \tag{E22}$$

So,

$$\varphi_0 \approx \varphi_\infty - \frac{\beta \rho^{\text{in}} R^2}{2 M_{pl}} = \varphi_\infty - 3 \beta M_{pl} \Phi_N \ . \tag{E23}$$

Finally,

$$\varphi_{\text{thick}}^{\text{out}}(r) \approx -\frac{\beta \rho^{\text{in}} R^3}{3 M_{pl}} \frac{e^{-m_{\text{eff}}^{\text{out}} r}}{r} + \varphi_\infty \tag{E24}$$

$$= -\frac{\beta \mathcal{M}}{4 \pi M_{pl}} \frac{e^{-m_{\text{eff}}^{\text{out}} r}}{r} + \varphi_\infty \qquad (R \leq r) \ . \tag{E25}$$

Thus, when comparing this solution with the approximate solution for $\varphi_{\text{thin}}^{\text{out}}(r)$ we see that the r dependence of the *thick shell* exterior solution is *not* suppressed by the thin shell parameter.

In our approach, we always approximate the resulting effective potentials (in each of the various bodies and surrounding media present in the problem) up to quadratic order in φ around their corresponding minima. Thus, our effective potential is described, in each region by quadratic expressions in φ, for the whole domain $\mathbb{R}^3$.

In particular, inside the body $0 < r < R$ we use a single quadratic expression while, as mentioned above, in the KW approach, the potential is taken to be linear in φ in the region $R_{\text{roll}} < r < R$. Furthermore, in order to determine which of the two approximations is better we rely on the energy functional criteria described in section III which takes into account the exact form of the effective potential. It follows from the results of Section III that when the large body does not satisfy the *thin shell* condition as characterized within the standard approach, the latter approximation to the effective potential is better than ours. In a future work [26] we will consider an adaptive method interpolating between the two approximations and use the energy criteria developed in this work to establish if does it provide a better approximation for all values of the parameters.

[1] J. Khoury, and A. Weltman, Phys. Rev. Lett. **93**, 171104 (2004); Phys. Rev. D **69**, 044026 (2004)

[2] R. Wald, Phys. Rev. D **6**, 406 (1972)

[3] A. Papapetrou, Proc. R. Soc. London A **209**, 248 (1951); E. Corinaldesi, and A. Papapetrou, Proc. R. Soc. London A **209**, 259 (1951); W. G. Dixon, Proc. R. Soc. London A **314**, 499 (1970)

[4] I. T. Drummond, and S. J. Hathrell Phys. Rev. D **22**, 343 (1980)

[5] J. D. Bekenstein, Phys. Rev. D **25**, 1527 (1982)

[6] J. D. Barrow, J. Magueijo, and H. B. Sandvik, Phys. Rev. D **66**, 043515 (2002)

[7] K. A. Olive, and M. Pospelov, Phys. Rev. D **65**, 085044 (2002)

[8] T. Damour, and A. M. Polyakov, Nuclear Physics B **423**, 532 (1994)

[9] G. A. Palma, P. Brax, A. C. Davis, and C. van de Bruck, Phys. Rev. D **68** 123519 (2003)

[10] E. G. Adelberger et al., Prog. in Particle and Nuclear Physics **62**, 102 (2009)

[11] P. G. Roll, R. Krotkov, and R. H. Dicke, Ann. Phys. (N. Y.) **26**, 442 (1964)

[12] V. B. Braginski, and V. I. Panov, Sov. Phys. J. E. T. P. **34**, 463 (1972)

[13] G. M. Keiser, and J. E. Faller, Proc. $2^n d$ Marcel Grossman Meeting on General Relativity", p.696 (1982)

[14] Y. Su et al., Phys. Rev. D **50**, 3614, (1994)

[15] S. Schlamminger et al., Phys. Rev. Lett. **100**, 041101 (2008)

[16] T. Damour, F. Piazza, and G. Veneziano, Phys. Rev. Lett. **89**, 081601 (2002)

[17] K. A. Olive, and M. Pospelov, Phys. Rev. D **77**, 043524 (2008)

[18] P. Brax, C. van de Bruck, A. C. Davis, J. Khoury, and A. Weltman, Phys. Rev. D **70**, 123518 (2004)

[19] D. F. Mota, and D. J. Shaw, Phys. Rev. D **75**, 063501 (2007)

[20] P. Brax, C. van de Bruck, A. C. Davis, D. F. Mota,and D. Shaw, Phys. Rev. D **76**, 124034 (2007)

[21] L. Hui, A. Nicolis, and C. W. Stubbs, Phys. Rev. D **80**, 104002 (2009)

[22] P. Brax, C. van de Bruck, D. F. Mota, N. J. Nunes, and H. A. Winther, Phys. Rev. D **82**, 083503 (2010)

[23] P. Brax, and C. Burrage, Phys. Rev. D **83**, 035020 (2011)

[24] P. Brax, A. C. Davis, B. Li, and H. A. Winther, Phys. Rev. D **86**, 044015 (2012)

[25] A. Upadhye, Phys. Rev. D **86**, 102003 (2012)

[26] L. Kraiselburd, S. J. Landau, M. Salgado, D. Sudarsky, and H. Vucetich, (in preparation)

[27] J. Khoury, Class. Quantum Grav. **30**, 21 (2013)

[28] T. Tamaki, and S. Tsujikawa, Phys. Rev. D **78**, 084028 (2008)

[29] K. Saaidi, and A. Aghamohammadi, Astrophysics Space and Science **333**, 327 (2011)

[30] D. Puetzfeld, and Y. N. Obukhov, Phys. Rev. D **92**, 081502 (2015)

[31] L. Kraiselburd, S. J. Landau, M. Salgado, D. Sudarsky, and H. Vucetich, (in preparation)

[32] G. Kristensson, Course of Electromagnetic Wave Propagation, Faculty of Engineering, Lund University (2008)

[33] J. Bruning, and Y. Lo, IEEE Trans. Antennas Propagat., **19**, 378-390 (1971)

[34] N. Gumerov, and R. Duraiswami, J. Acoust. Soc. Am. **112**, 2688 (2002)

[35] N. Gumerov, and R. Duraiswami, SIAM J. Sci. Comput. **25**, 1344 (2003)

[36] C. M. Will, Living Rev. Relativity **17**, 4 (2014)

[37] E. G. Adelberger et al., Phys. Rev. D **42**, 3267 (1990).

[38] S. J. Landau et al., Astropart. Phys. **35**, 377-382 (2012)

[39] P. Hamilton, M. Jaffe, P. Haslinger, et al., Science **349**, 849 (2015)

[40] S. Schlögel, S. Clesse, and A. Füzfa, Phys. Rev. D **93**, 104036 (2016)

[41] B. Elder, J. Khoury, P. Haslinger, et al., Phys. Rev. D **94**, 044051 (2016)

[42] C. Burrage, and J. Sakstein, arXiv:1609.01192 (2016)

[43] C. Burrage, E. J. Copeland, and E. A. Hinds, JCAP, **03**, 042 (2015)

[44] T. W. Murphy, Reports on Progress in Physics **76**, 076901 (2013)

[45] R. Gannouji et al., Phys. Rev. D **82**, 124006 (2010)

[46] V. Vikram, J. Sakstein, C. Davis, and A. Neil, arXiv:1407.6044 (2014)

[47] A. Terukina, L. Lombriser, K. Yamamoto, et al., JCAP, 4, 013 (2014)

[48] H. Wilcox, D. Bacon, R. C. Nichol, et al., MRAS, 452, 1171 (2015)

[49] B. Jain, V. Vikram, and J. Sakstein, Astrophys. J. , 779, 39 (2013)

[50] T. Jenke, G. Cronenberg, J. Burgdörfer, et al., Phys. Rev. Lett. **112**, 151105 (2014)

[51] W. Hu, and I. Sawicky, Phys. Rev. D **76**, 064004 (2007); T. Faulkner, M. Tegmark, E. F. Bunn, and Y. Mao, Phys. Rev. D **76**, 063505 (2007); S. Capozziello, and S. Tsujikawa, Phys. Rev. D **77**, 107501 (2008); P. Brax, and C. van de Bruck, and A.C. Davis and D.J. Shaw, Phys.Rev. D **78**, 104021 (2008); L. Lombriser, F. Simpson, and A. Mead, Phys. Rev. Lett. **114**, 251101 (2015)

[52] T. P. Waterhouse, astro-ph/0611816 (2006)

[53] Bergé, J., Touboul, P., Rodrigues, M., & MICROSCOPE Team 2015, Journal of Physics Conference Series, 610, 012009